PLASMA ELECTROLYTIC OXIDATION OF TITANIUM

UNDER CONSTANT APPLIED VOLTAGE

by

JOSHUA TWADDLE

Presented to the Faculty of the Graduate School of

The University of Texas at Arlington in Partial Fulfillment

of the Requirements

for the Degree of

MASTER OF SCIENCE IN MATERIALS SCIENCE AND ENGINEERING

THE UNIVERSITY OF TEXAS AT ARLINGTON

May 2020

ACKNOWLEDGEMENTS

Firstly, I must express my sincerest gratitude to my advising professor Dr. Efstathios Meletis. His leadership provided continuous encouragement and support throughout my studies and into my research, while his knowledge offered a seemingly limitless supply of helpful guidance and advice as I grew academically. I would also like to extend thanks to the other members of my research committee: Dr. Jiechao Jiang, and Dr. Ye Cao for their advice and their overwhelming assistance with my project.

Next, I would like to thank some of my closest friends from UTA. Brody, Hooman, Ignacio, Allison, and Ben, you guys are like family to me. Each of you has managed to help me with my studies be it group study sessions to prepare for a class or making the hour-long commute to campus not seem so long. I am truly in your debts.

Finally, my dearest thanks go out to my family. Your unwavering love and support provided me with the confidence to challenge any task put in front of me. Each of you inspires me every day to be a better man and every milestone should act as a testament to the incredible family I have supporting me.

May 3, 2020

ABSTRACT

PLASMA ELECTROLYTIC OXIDATION OF TITANIUM

UNDER CONSTANT APPLIED VOLTAGE

Publication No. _____

Joshua Twaddle; M.S.

The University of Texas at Arlington, 2020

Supervising Professor: Dr. Meletis

Plasma Electrolytic Oxidation (PEO) is a method capable of applying nonmetallic coatings to metallic substrates submerged in electrolyte via a plasma development under high voltage. The PEO technique is particularly useful in the coating of materials such as Ti-, Al-, and Mg-based alloys. In this study, the effects of varying processing voltage and time on oxide coating characteristics formed on pure titanium surfaces was investigated.

First, it was necessary to confirm that the selected electrolyte type and concentration could produce PEO coatings in a predictable fashion. Experiments were performed with constant current density by constantly controlling the voltage, so the results could be compared and complement

previous experiments performed on the same substrate. It was discovered that the new electrolyte produced arcing, having an adverse effect on coating quality. A similar relationship between current density and time was obtained, as in the previous experiments, so it was concluded that the new electrolyte was adequate. Experiments were then performed at a wide voltage range with the voltage being manually increased to and then held constant at desired values to study the current density behavior. These observations indicated that current density remains high early in the process where high voltage values prevail, and then decays quickly (almost to zero). Thus, a higher initial voltage leads to longer processing times before the current dies out. It was hypothesized that the amount of charge (current density x time) is indicative of coating thickness. As shown in previous works, the coating thickness is dependent on the ionic current applied to the sample, which makes up only part of the total current density. This ionic current makes up no more than half of the total current density and decreases to zero at current densities below 30 mA/cm^2. Through these experiments it was discovered that a higher operating potential allowed for continued ionic current application for longer time spans during processing. For this reason, a potential of 450 V was selected for additional experiments. Several methods of characterization were used to identify the effects of varying processing voltages and processing time on the roughness, morphology, composition, and thickness of the applied oxide coating. Processing voltage was found to be the only characteristic that effected coating thickness, and processing time was found to only have a pronounced effect on the composition of the coating while the other characteristics remained unchanged. Through this project, it was discovered that using the constant voltage method of PEO, the maximum amount of ionic current that can be applied (and therein the maximum coating thickness) can be reached within a minute of processing. The changes in coating composition as a function of coating thickness were also determined.

TABLE OF CONTENTS

LIST OF ILLUSTRATIONS

LIST OF TABLES

CHAPTER 1

INTRODUCTION

1.1 Introduction & Motivation

A common issue found in the aerospace, automotive, and biomedical industries is the need for a lightweight, corrosion-resistant material that has acceptable wear resistance. Titanium and titanium alloys offer a particularly high strength to weight ratio. Due to the natural formation of oxide on the surface, they also have substantial corrosion resistance and biocompatibility [1]. This combination of characteristics has led to the popularity of titanium and its alloys as materials in everything from cars to implants. Unfortunately, pure titanium and titanium alloys suffer from a lack of wear resistance. One method of efficiently improving the wear resistance of titanium substrates is applying a coating to the surface, which has made the study of coating titanium a necessary area of research [2].

Research has been performed using a wide range of methods to apply surface coatings to titanium substrates in order to improve their tribological characteristics. These methods include physical vapor deposition, sol-gel application, ion sputtering, electrocyrstallization, etc. [1,3,4]. Each of these processes have their own distinct advantages, but, in the last decade, PEO has emerged as perhaps the most beneficial method to applying tough coatings with improved mechanical characteristics and adhesion strength.

Presently, there have been a sizable number of research projects geared towards increasing our understanding of PEO and its mechanism on metallic substrates [2, 5-6]. Mortazavi et al. [2] worked to improve the understanding of PEO using titanium substrates. They studied the outcome of experiments performed with constant current density. Processing at a constant current density

requires the constant increase of voltage. As a coating is formed and increases in thickness, a higher voltage is required to maintain the same current density. Under these conditions, they were able to identify the breakdown voltage (minimum voltage at which plasma occurs), which was about 275 V. They were also able to indicate how certain electrolyte compositions affect the properties of the produced coating. Both discoveries were helpful in setting up the experiments performed in this study. In continuation with the results found using the constant current density method, this project aims to continue improving the understanding of the PEO mechanism by instead observing the behavior of current density decay when performed under constant voltage. Additionally, the cumulative results of both projects are currently utilized by our group in the Surface and Nano Engineering Lab (SaNEL) with the goal to accurately model the PEO mechanism by predicting the coating thickness under constant voltage and current density.

1.2 Research Objectives

The research objectives of this present project are:

- Study the effects of current density-time (i-t) behavior under constant voltage. This is performed by processing an array of titanium samples at varying voltages and recording the current density decay with time.

- Assess the effects of processing time and voltage on the coating thickness, composition, and surface morphology. This is accomplished by characterizing the processed substrates using cross-sectional metallography, profilometry analysis, X-ray diffraction analysis (XRD), scanning electron microscopy (SEM), and energy dispersive spectroscopy (EDS).

- Contribute to the understanding of the PEO mechanism by observing the decay of ionic current as a function of decaying current density under throughout the constant voltage PEO processing.

CHAPTER 2

LITERATURE REVIEW

2.1 Titanium & Titanium Oxide

Titanium is one of the most abundant metals on Earth, but, due to its lower toughness and melting temperature, its use in structural applications is eclipsed by copper and iron. Commercial production of titanium metal exploded in 1948 when it was first utilized by the aerospace industry. Naturally occurring minerals that contain titanium include rutile, leucoxene, and ilmenite, which supplies over 90% of the world's demand for titanium minerals [7]. Table 2.1 below shows a list of titanium minerals compared alongside their composition and percent titanium dioxide content.

Table 2.1: Titanium Minerals and Their Chemical Makeup [7]

Mineral	Composition	TiO_2 content (%)
Rutile	TiO_2 (tetragonal, twinned)	~95%
Anatase	TiO_2 (tetragonal, near octahedral)	~95%
Brookite	TiO_2 (orthorhombic)	~95%
Ilmenite	$FeO \cdot TiO_2$	40–65%
Leucoxene	$Fe_2O_3 \cdot nTiO_2$	>65%
Arizonite	$Fe_2O_3 \cdot nTiO_2 \cdot mH_2O$	–
Perovskite	$CaTiO_3$	–
Geikielite	$MgTiO_3$	–
Titanite or sphene	$CaTiSiO_5$	–
Titaniferous magnetite	$(Fe \cdot Ti)_2O_3$	–

The largest consumer of titanium dioxide is the pigment industry, which discovered that when the average particle size of TiO_2 particles is below 100 nm, the compound begins to develop unique optical iridescence. This quality of TiO_2 gives it the ability to be used in cosmetics, ceramics, and percaline industries as popular additives [7]. The samples used, however, were not obtained in this manner, but were instead cut from a sheet of commercially pure titanium. Table 2.2 shows the chemical composition and diffusion information of commercially pure titanium.

Table 2.2: Composition and Diffusion Information of CP-Ti [8]

Element	Composition (p.p.m.)	Activation energy, volume diffusion, Q (kJ/mol)	Frequency factor, D_0 (m^2/s)
C	18	182.1	$5.0! \times 10^{-4}$
N	6	228.2	$2.9! \times 10^{-5}$
O	270	200.9	$4.5! \times 10^{-5}$
H	1	46.1	$1.15! \times 10^{-6}$
Fe	6	144.2[a]	$6.4! \times 10^{-6a}$
		112.3[b]	$4.7! \times 10^{-7b}$
S	2		
Ti	balance	192.8	$1.74! \times 10^{-8}$

[a] Perpendicular to the c-axis.
[b] Along the c-axis.

Titanium can form a wide variety of oxides other than the most common, TiO_2. The work of Murray et al. [9] studied the oxide phases that exist between titanium and titanium dioxide. Oxides formed in this region can be categorized into 5 phases. The β-Ti_2O_3 and rutile phases both showed congruent melting behaviors and melted at higher average melting temperatures. The γ-TiO, β-Ti_3O_5, and γ-Ti_4O_7 phases instead melted unevenly, and at significantly lower temperatures. Their research produced a useful graphical representation of the relationship between titanium and oxygen in the form of a phase diagram shown below as Figure 2.1. As this graph illustrates, the melting point of Ti-O compounds range from about 1650-1925 °C.

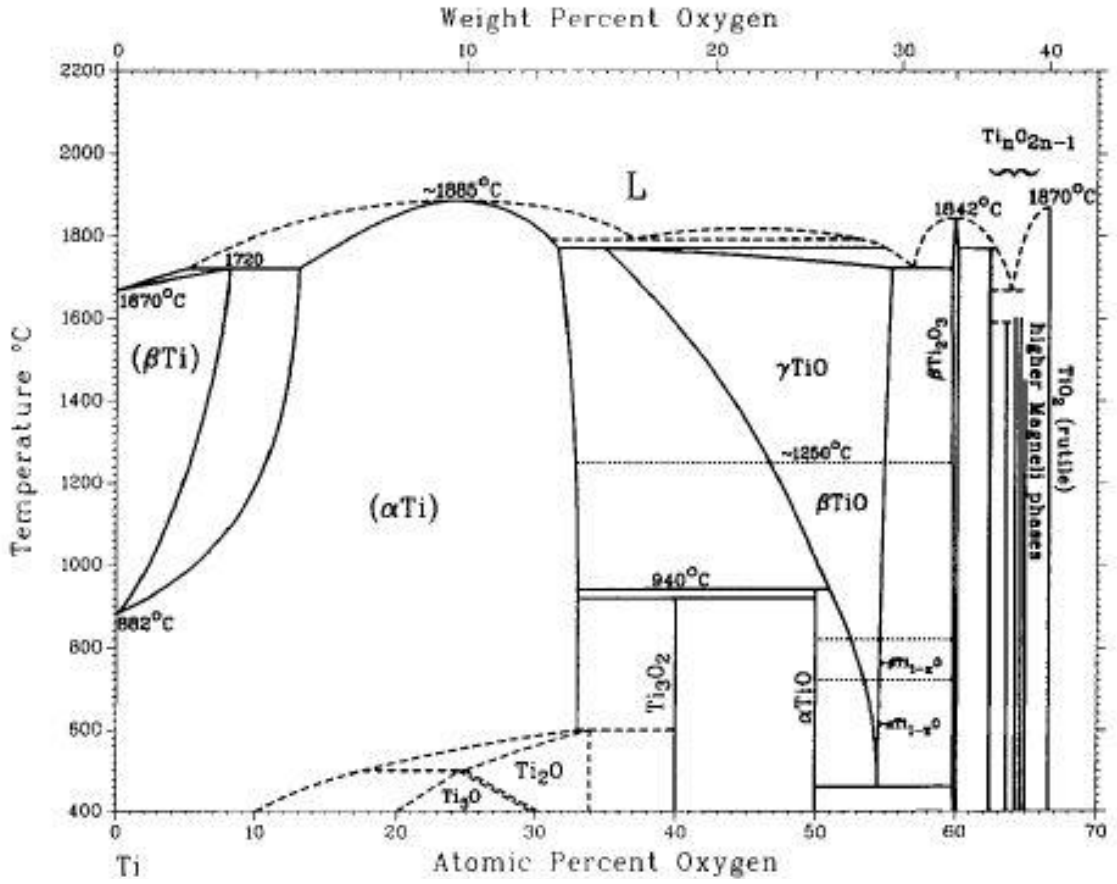

Figure 2.1: Ti-O Phase Diagram [9]

2.2 Plasma Electrolytic Deposition:

Plasma electrolytic deposition (PED) is becoming an increasingly popular method for surface modification. Despite being first demonstrated half a century ago, plasma deposition has competitive attributes. High deposition rate allows for coatings to be applied efficiently, while the excellent adhesion helps assure minimal thin-film fracture. Methods for application of coatings through more traditional chemical reactions carry with them the potential to harm the surrounding environment if not properly disposed, particularly in the application of metals. Plasma deposition

can be used to apply both nonmetallic and metallic coatings whilst remaining ecologically friendly [10]. The application of this method into industry is presently minimal, but as the knowledge of the mechanism and potential applications come to light, its benefits are likely to lead to more frequent utilization. A basic schematic for the mechanism of PED is shown below in figure 2.2.

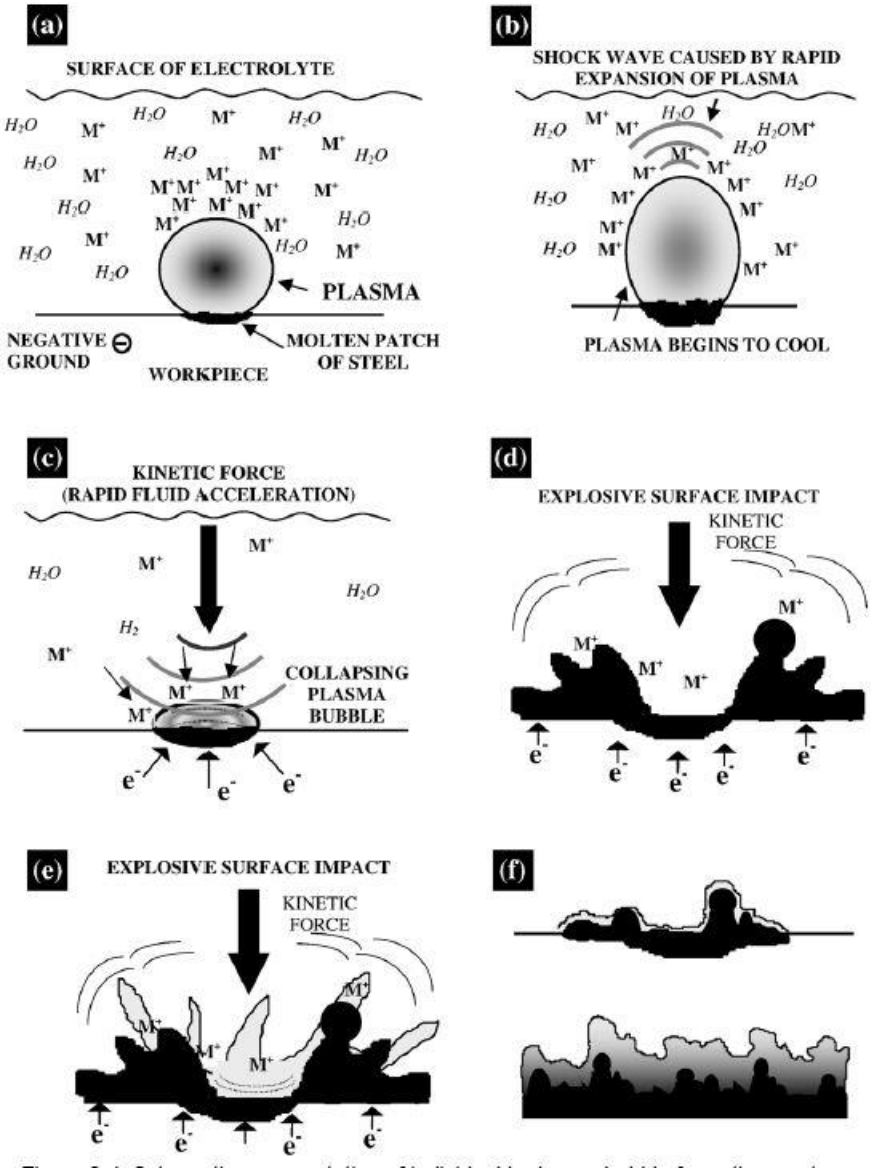

Figure 2.2: Schematic for the Mechanism of PED [10]

PED can be categorized into two groups based on the direction of current flow. In electrolytic plasma processing (EPP), the working electrode acts as the cathode. EPP is the most ideal process for the cleaning of, or application of a metal coating to, the surface of the substrate [11].

Alternatively, when the working electrode is used as the anode in the cell, non-metals can be applied. This process is known as Plasma Electrolytic Oxidation.

2.3 Plasma Electrolytic Oxidation

PEO is becoming an increasingly popular method of treating titanium and its alloys, because the clean application of a nonmetallic coating can drastically improve the surface properties [12]. To conduct PEO, an electrochemical cell must be created using an electrolyte with known pH and electrical conductivity [13]. The metal substrate is then submerged in the cell surrounded by a counter electrode. The sample acts as the anode as a large voltage is applied, and once the voltage goes beyond the breakdown potential, sparks begin appearing on the surface. These small sparks locally melt the surface of the sample while the surrounding electrolyte is water cooled to maintain a reasonable temperature. As the surface is melted, ions from within the electrolyte react and bond with the metal. Finally, when the reaction finishes and the potential is returned to zero, the surface of the substrate returns to a solid with the new coating applied to its

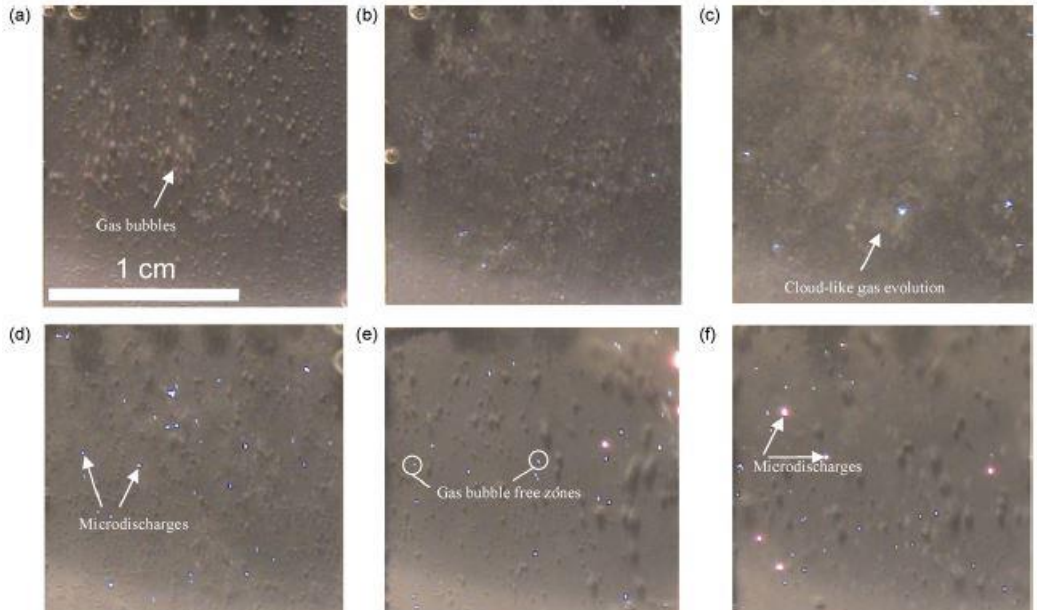

Figure 2.3: Images Taken During PEO at a) 273V; b) 300V; c) 350V; d) 405V; e) 430V; f) 435V [15]

surface. Figure 2.3 shown above are images taken of the surface of samples during the PEO process performed at different voltages. Additionally, Figure 2.4 illustrates the PEO process discharging behavior.

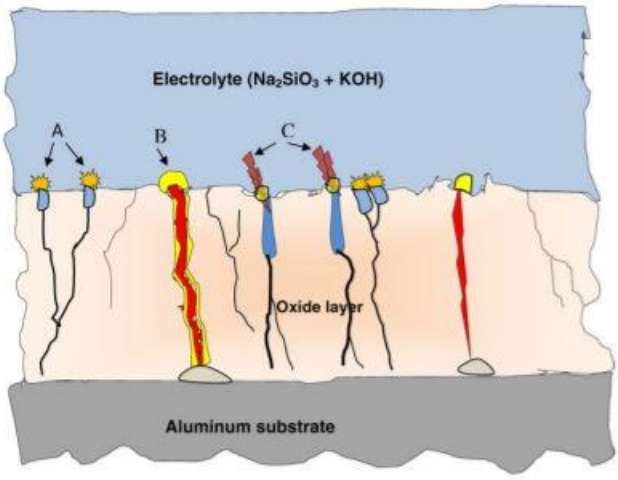

Figure 2.4: PEO Process Discharge Behavior

In PEO there are two currents applied to the surface that need to be considered. The first is the electric current, which primarily causes the sparking and the heating of the surface. Second is

the ionic current, which provides the largest contribution to the growth of oxides as it provides the ions with which the coating is formed. Mortazavi's work in the SaNEL Lab [2] also led to the increased understanding of the relationships these currents play in the PEO mechanism. Through performing constant current density experiments and observing the charges, they were able to deduce that the ratio of ionic current contribution to the total current density increases with increasing total current density in a near-linear behavior. These results are shown below as Figure 2.6.

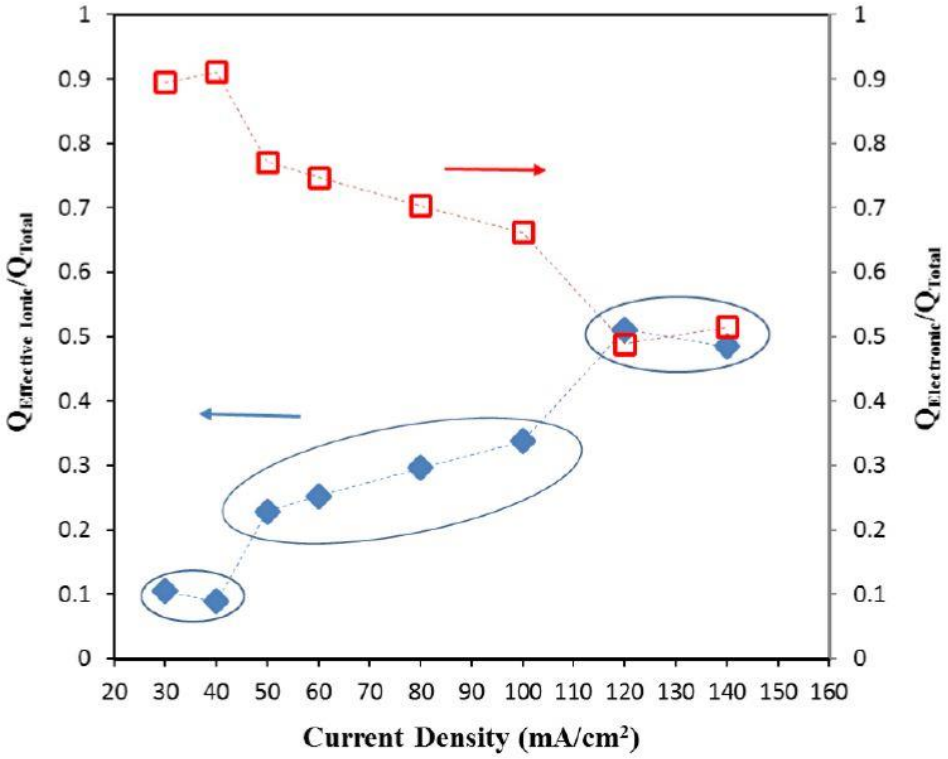

Figure 2.6: Ionic and Electronic Current Contribution at Various Current Densities [2]

In Shokouhfar et al. [16], the effects of various electrolytes at varied concentrations on the coating and corrosion resistance of the oxide formed via PEO were studied. They found that any adjustment in the electrolyte composition led to a change in the porosity of the coating, and that

phosphate containing electrolyte produced the most corrosion resistant coatings. This led to the use of phosphorus-based electrolytes in this experiment. Jung et al. [17] also studied the effects of certain electrolytes on the PEO process with titanium. They showed great success forming thick coatings using potassium ions in the electrolyte. This information led to the use of potassium hydroxide as the added base to the electrolyte. The work of Venkateswarlu et al. [18] used borate, silicate and citrate as possible electrolyte components when performing PEO on Titanium, while these chemicals weren't used in this project, they did indicate that very little electrolyte concentrations were required to get the desired result, which allowed for less chemical waste when running experiments.

Most of the studies that have already been performed focused on the effects of alternate electrolyte compositions or titanium alloys, or they focus on performance at constant or pulsed current density. Studying the effects of different parameters under constant voltages will provide a unique perspective that will aid in the understanding of the PEO mechanism. It will also outline the relevancy of said parameters when developing the nonmetallic coating.

CHAPTER 3

EXPERIMENTAL STUDY

3.1: Materials

The substrates used in this study were rectangular strips of CP Ti (25 x 15 x 0.5 mm) with long rectangular tails to secure each sample to the rod that would connect the sample to the anodic current. Before processing, the tails of each sample were insulated with tubing, so that the reaction would be limited to the larger rectangular piece. These processing regions had surface areas averaging about 5.11 cm^2.

3.2 Processing Procedure

A double wall reaction vessel setup like the one used for these experiments is shown below in figure 3.1. The first stage of preparing the PEO setup was to attach two rubber tubes to the

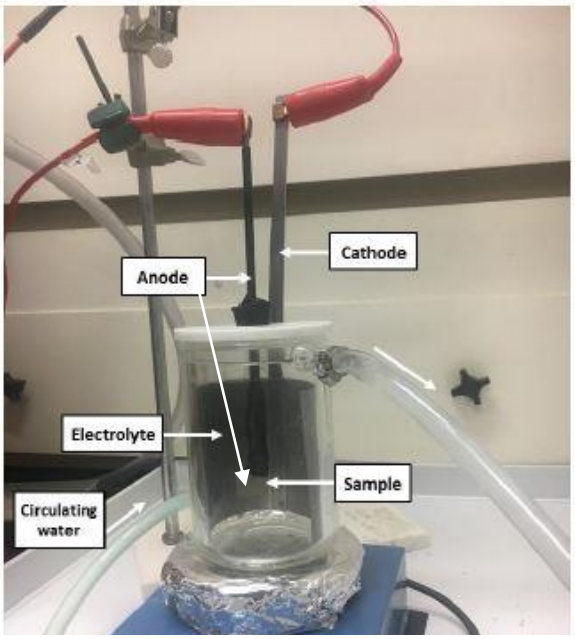

Figure 3.1: Example of Similar Reaction Vessel [12]

double-walled beaker. The tube connecting to the lower input on the beaker was also fastened to the feedthrough to provide water cooling, while the tube connected to the higher output leads the warm water to the drain. A stir bar is then inserted into the beaker along with 300 mL of deionized water to begin the mixing of the electrolyte. For the correct pH and conductivity, 0.9910 g of potassium pyrophosphate and 0.0337 g of potassium hydroxide (give or take 5 ten thousandths of a gram) must be added to the 300 mL of DI water. This makes the approximate concentration of $K_4P_2O_7$ 0.01 M and the concentration of KOH about 0.02 M. The stir bar was then spun by the hot plate to aid in the dissolving of the added chemicals. While waiting on the homogeneity of the electrolyte, the working electrode was insulated, attached to the insulated rod, and the rod attached to the lid that was made to fit securely to the top of the beaker. The insulation was used to ensure that only the rectangle at the bottom of the working electrode was processed. Once the electrolyte was prepared, the stainless-steel counter electrode, which wraps around three quarters of the beaker wall to ensure the surrounding of the working electrode and give space to observe the reaction, is placed firmly within the beaker. The lid with the accompanying working electrode were then placed on top with the electrode faces directed towards the counter electrode on both sides. This is one aspect that was changed from the previous works to help increase the overall coating application.

With the reaction vessel complete, the power source could be connected, and the processing performed. Since PEO is the anodic form of PED, the positive electrode was attached to the conductive rod connected to the sample, while the negative electrode was attached to the counter electrode. Another change from previous experiments performed in this vessel was the location at which the counter electrode was attached. The image shown portrays it connected at the top near the spot where the anode was connected. This, however, was deemed to be a potential risk given

the potential difference between the two clamps, so the cathode was bent away from the anode and clamped at half the initial height.

The first stage of the experiment was dedicated to running constant current density experiments with the applied changes to the reaction vessel and electrolyte volume from Mortazavi et al.'s experiments. Figure 3.2, shown below, illustrates the work done by Mortazavi's group to define the relationship between constant current density experiments. This was done to both ensure

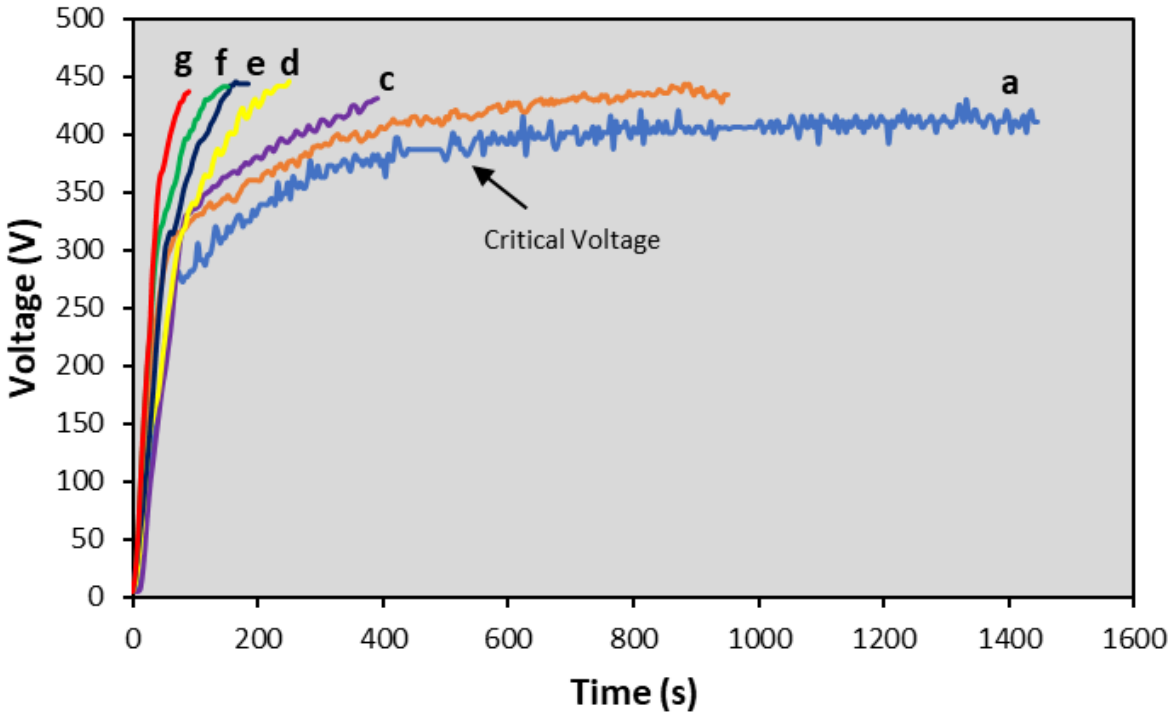

Figure 3.2: Voltage vs. Time Experiments Performed at Different Constant Current Densities: a) 30 mA/cm^2, b) 40 mA/cm^2, c) 50mA/cm^2, d) 60 mA/cm^2, e) 80 mA/cm^2, f) 100 mA/cm^2, g) 120 mA/cm^2

the experiment operated similarly to the previous setup, and to illustrate that the processing time at which the current density could be maintained experimentally increased with decreasing constant current density.

Once constant current density experiments were completed, the project shifted to working exclusively with constant processing voltage. To determine which processing voltage was likely

to produce the largest coatings, the graphs of current density vs. time were created for samples processed at 300, 350, 400, and 450 V. The graphs were used to calculate the processing time at which the ionic current decayed to zero, which indicates no further coating is being formed. The voltage at which the longest maintained ionic current was achieved was then selected as the constant voltage for ongoing experiments. Samples were then compared after being processed at 10, 20, 50, and 100 s. To show the effect of processing time on roughness, five points (one at each corner, and one at the center) from each of the four samples were examined by profilometry. Two strips were then obtained from each sample. The strips were pressed together using a stainless-steel clip, and then mounted in Bakelite. Following mounting, they were thoroughly polished so the cross-section of each sample could be studied and then examined under a scanning electron microscope. Energy dispersive spectrometry line-scans were also performed in tandem with the SEM images to help elucidate the coating thickness. For the 10 s and 100 s processing times, the small remaining pieces of coated titanium were studied by X-ray diffraction. These results were combined in tandem with the SEM and EDS results to determine the structure and elemental composition of the formed coating.

3.3 Characterization Methods

3.3.1 Optical Profilometry

In order to obtain the roughness and an understanding of the surface morphology of the coatings that had been applied, white light interferometry through a profilometer was used. The relative smoothness of the surface meant that a 50x lens was required for quality results. Equation 3.1 written below shows the mathematical formula the program uses to calculate R_a.

Eq. 3.1 $$R_a = \frac{1}{n}\sum_{i=1}^{n}|y_i|$$

3.3.2 X-Ray Diffraction

XRD was used on two samples: the ones with the shortest and longest processing times. They were examined in θ-2θ mode for both samples, and from 20-80°. The accelerating current during the XRD was 40 mA, and the voltage was 40 kV. For maximum accuracy, an increment of 0.01° with a scan speed of 3 sec/step were used. The spectra were then vertically aligned so that common and unique peaks between them could be properly identified.

3.3.3 SEM & EDS

The topography and cross sections of the samples were analyzed using a Hitachi S-3000N SEM, and then for higher definition imagery, were studied using focused ion beam (FIB). All images from the SEM were obtained using an accelerating voltage of 25 keV, and with a working distance of about 15 mm. The images obtained were then analyzed to find and compare the average coating thickness and relative porosity from each of the samples from multiple groups of constant voltage experiments.

CHAPTER 4

RESULTS & DISCUSSION

4.1 Current Density – Time Response

The constant current density experiments were performed as the first stage of the experiment. Table 4.1 shows the results of the experiments run with the adjusted setup compared

Table 4.1: Comparison of Processing Times until Arcing at Different Constant Current Densities

Current Density (mA/cm^2)	**Mortazavi et al's Processing Time (sec)**	**Current Processing Time (sec)**
30	1446	240.2
40	950.2	103.8
50	390	23.6
60	250	22.0
80	184	21.6
100	152	15.8
120	90	10.6

to the results achieved by Mortazavi's group. The main characteristic used to verify the successful setup of the system was the increase in time before arcing with decreasing current density. This behavior was observed in the new experiments despite a large shift in processing times that must have been caused by the changes to the experiment setup.

Once that trend was confirmed, the experiment shifted to the constant voltage focus. The data from Mortazavi's group was used to create a new graph that illustrated what was to be

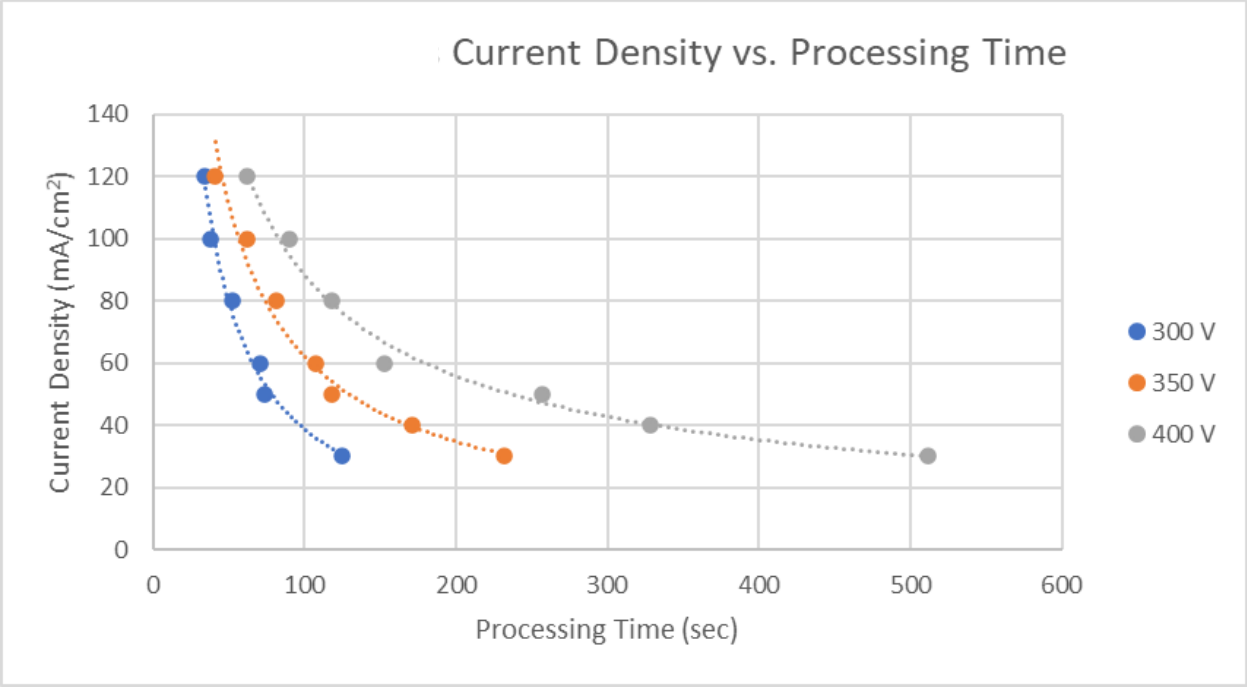

Figure 4.1: Mortazavi et al.'s Current Density vs. Time Response [12]

expected from current density – time relationship. Figure 4.1, shown below, shows the current density – time response that acted as a template for the experiments that followed. This pattern of increasing processing time with increasing constant voltage was found to be reproducible. Figure

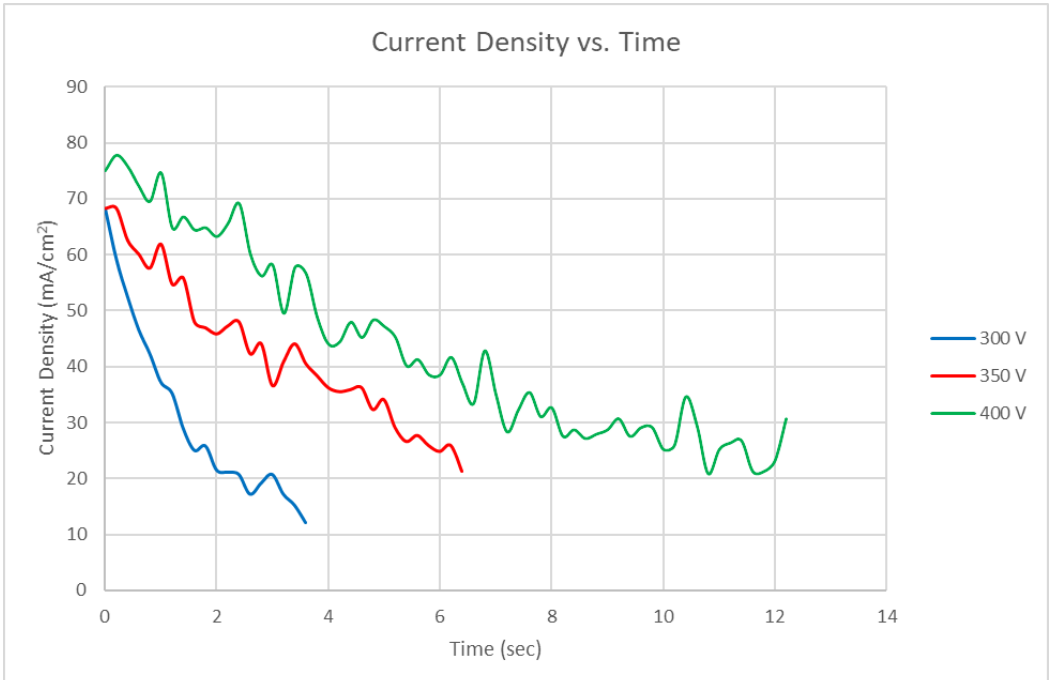

Figure 4.2: Current Density vs. Time Responses from 300, 350, and 400 V Constant Applied Voltage

4.2 shows the same pattern obtained with the new setup. The increase in variability likely comes from the faster rate of processing, but the maintained behavior allowed the project to continue.

The next goal was to determine the voltage that produced the thicker coating. Below are the Current Density vs. Voltage vs. Time graphs for experiments performed at 300, 350, 400, and 450 V.

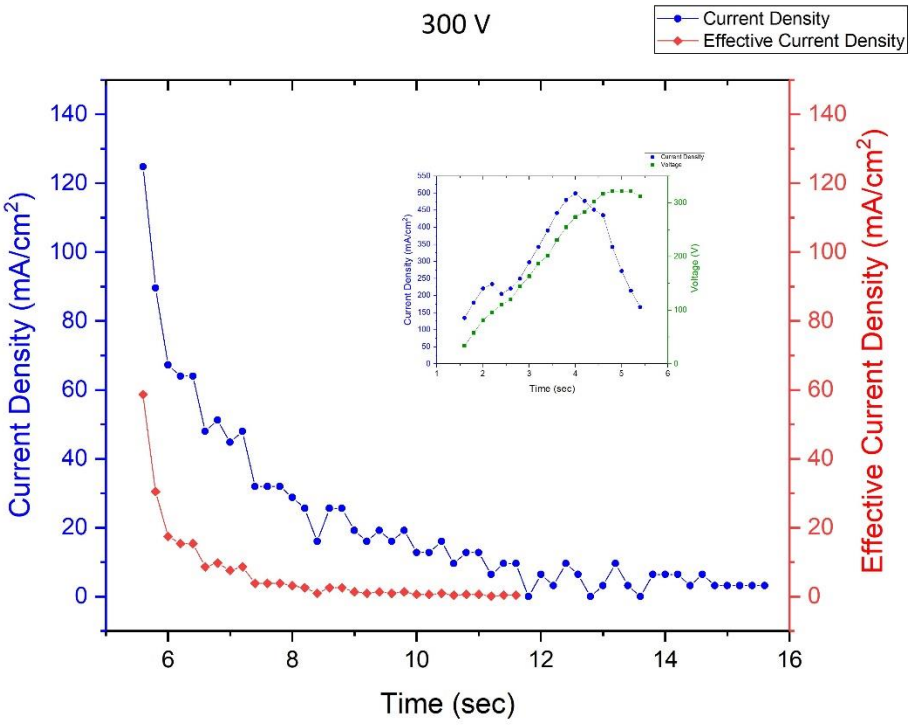

Figure 4.3: Current Density vs. Voltage vs. Time @ 300 V

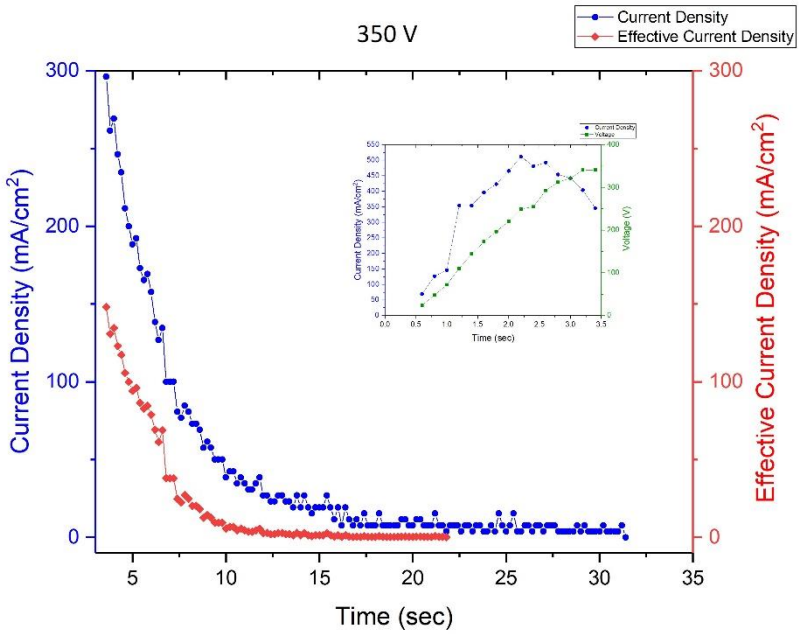

Figure 4.4: Current Density vs. Voltage vs. Time @ 350 V

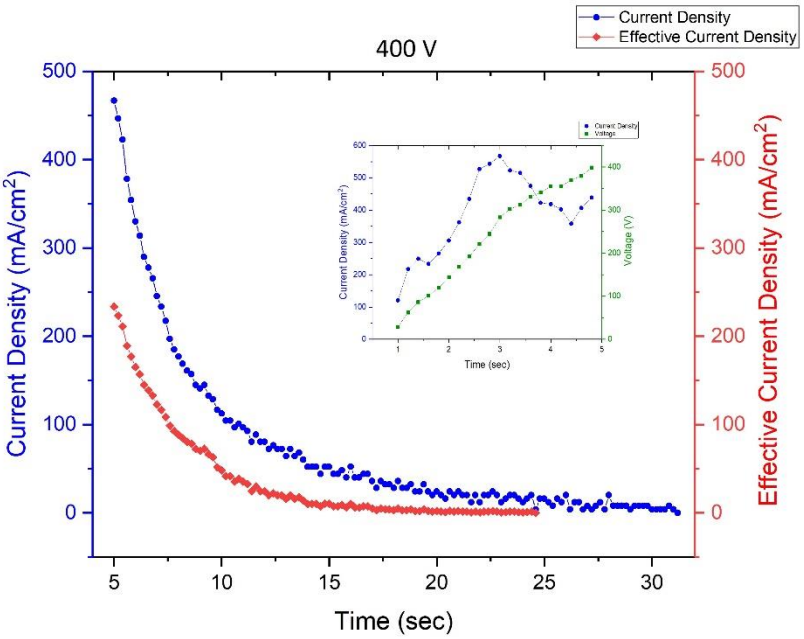

Figure 4.5: Current Density vs. Voltage vs. Time @ 400 V

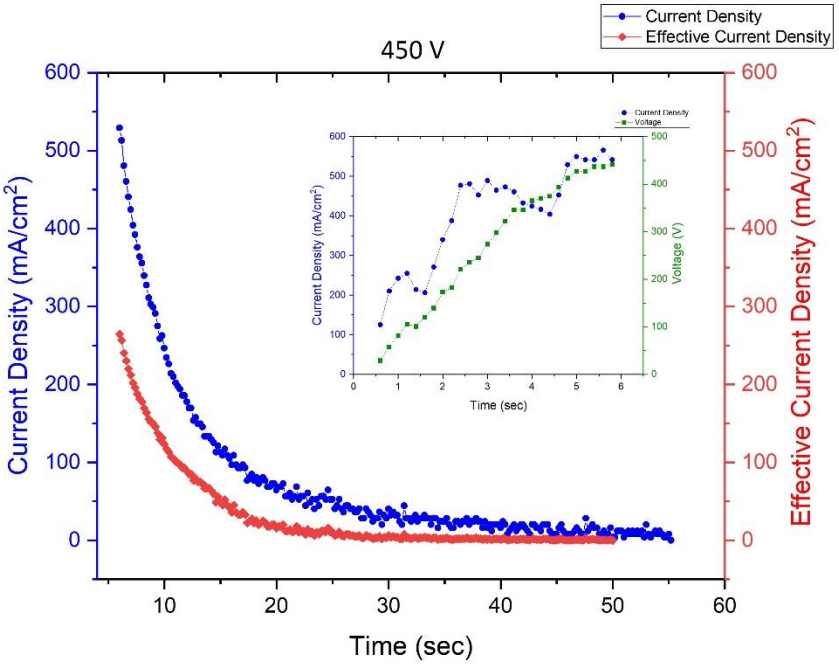

Figure 4.6: Current Density vs. Voltage vs. Time @ 450 V

As expected, the 450 V experiment had the longest time of maintained ionic current of 50 seconds and the largest processing time. Since the decay of ionic current could be more accurately studied over a larger span of time, this made 450 V ideal for further experiments. However, this also indicated that beyond about half a minute of processing the maximum coating thickness has already been applied, so very little coating thickness changes should be observed beyond that time.

To further describe the changes of coating application rate and the effects on surface characteristics changed with changing processing time, four new samples were processed at 450 V, but these samples had alternate processing times (10, 20, 50, and 100 s). Their current density vs voltage vs time responses are shown below.

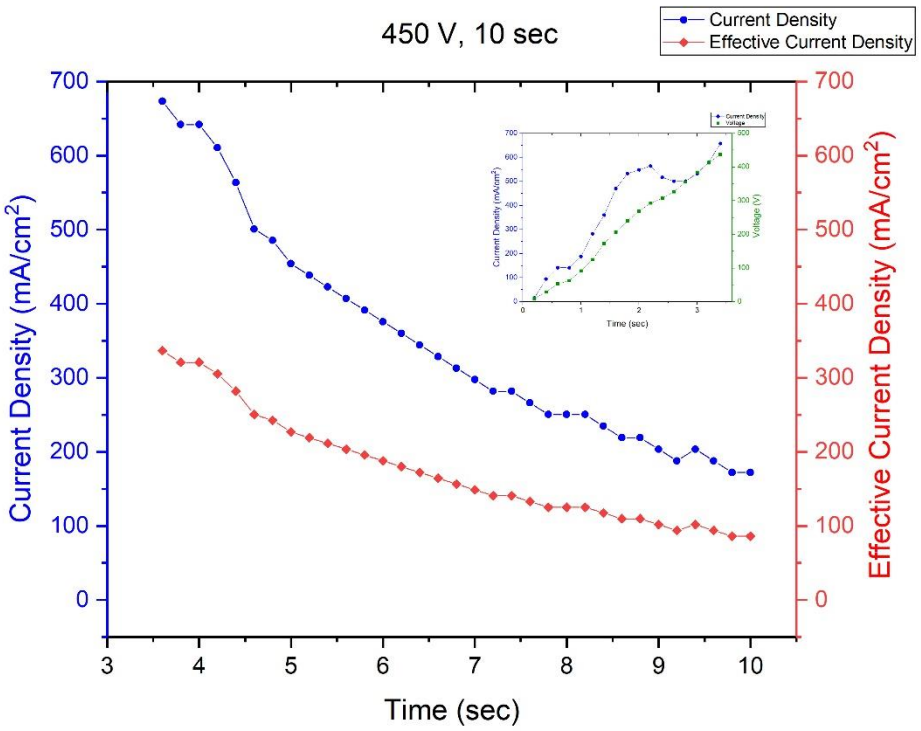

Figure 4.7: Total vs. Ionic Current Decay @ 450 V, 10 sec

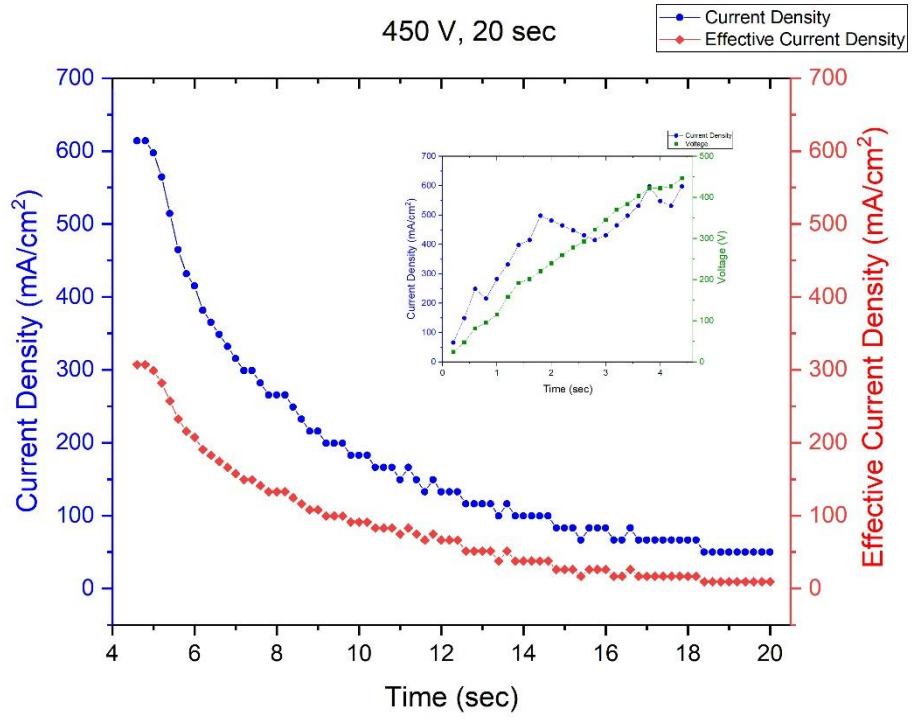

Figure 4.8: Total vs. Ionic Current Density Decay @ 450 V, 20 sec

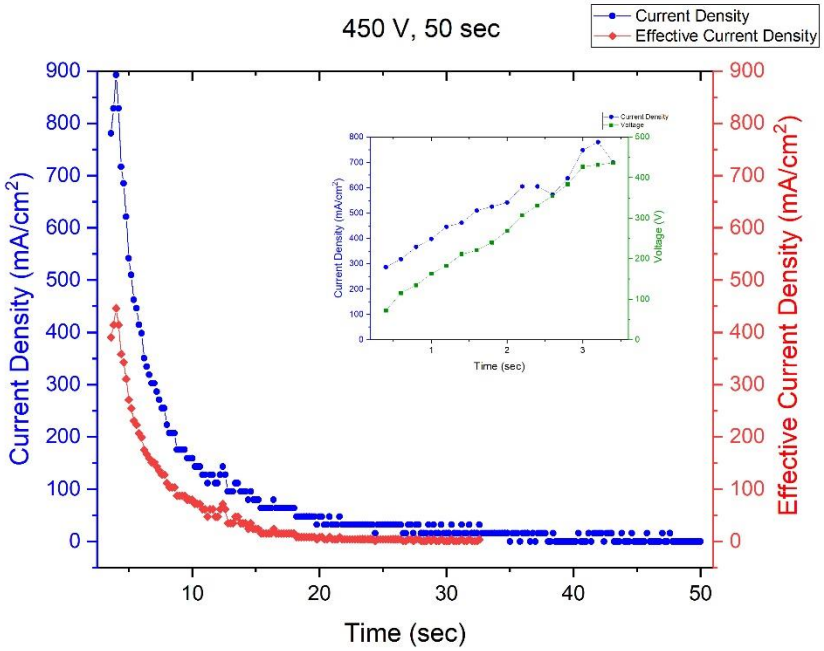

Figure 4.9: Total vs. Ionic Current Density Decay @ 450 V, 50 sec

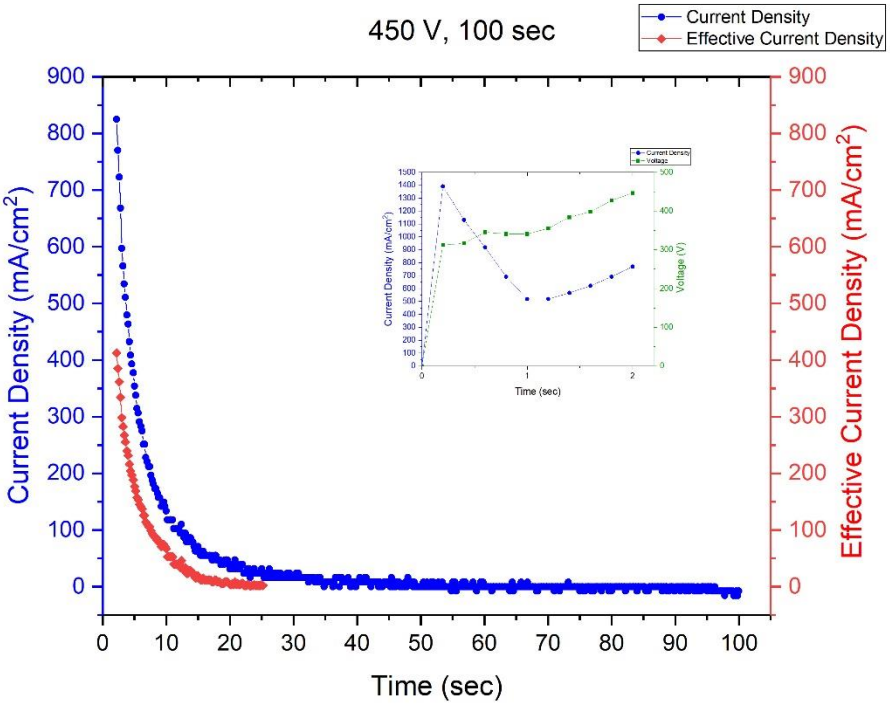

Figure 4.10: Total vs. Ionic Current Density Decay @ 450 V, 100 sec

These graphs indicate that despite the differences in processing time, the ionic current density only remains for about 30 seconds before decaying to zero. This shows that there should be no significant change in coating thickness between the 50 and 100 second processing times, and very little between them and the 20 second time, since ionic current density is the current that contributes the most to coating thickness.

4.2 Characterization

4.2.1 Profilometry Data

For the next stage, the same four processed titanium samples were taken to the profilometer to study any differences in roughness or surface morphology. Shown below are the results from the profilometer for the samples procured at 450 V.

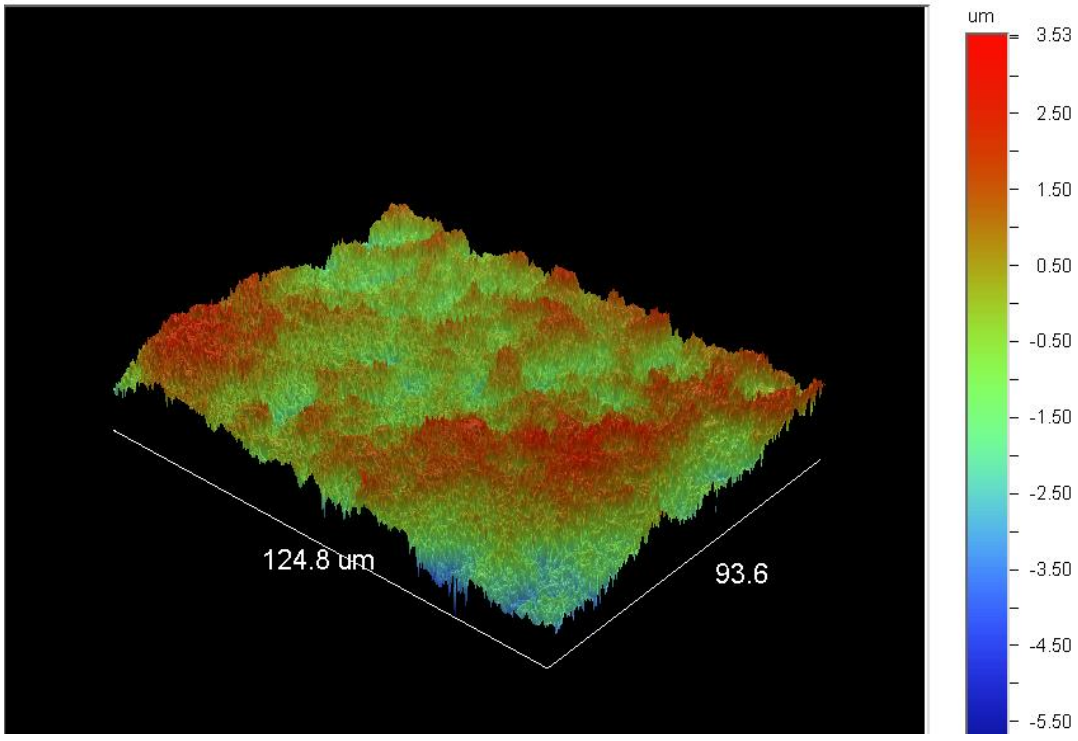

Figure 4.11: 3D Morphology 450 V, 10 sec

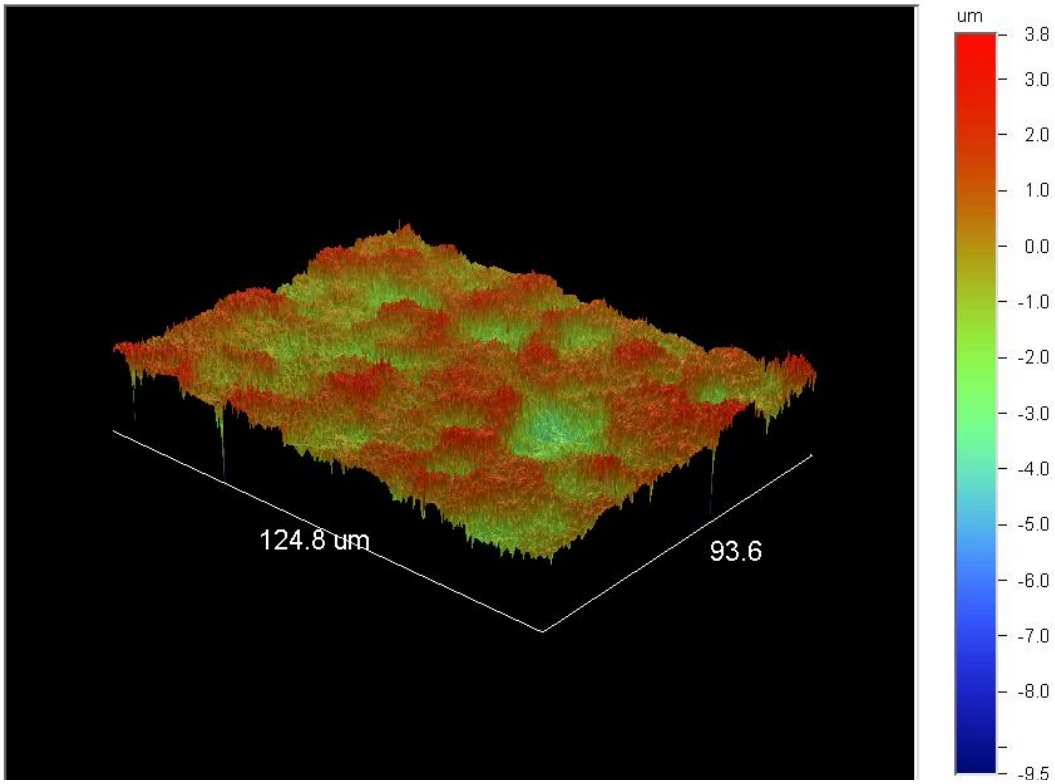

Figure 4.12: 3D Morphology 450 V, 20 sec

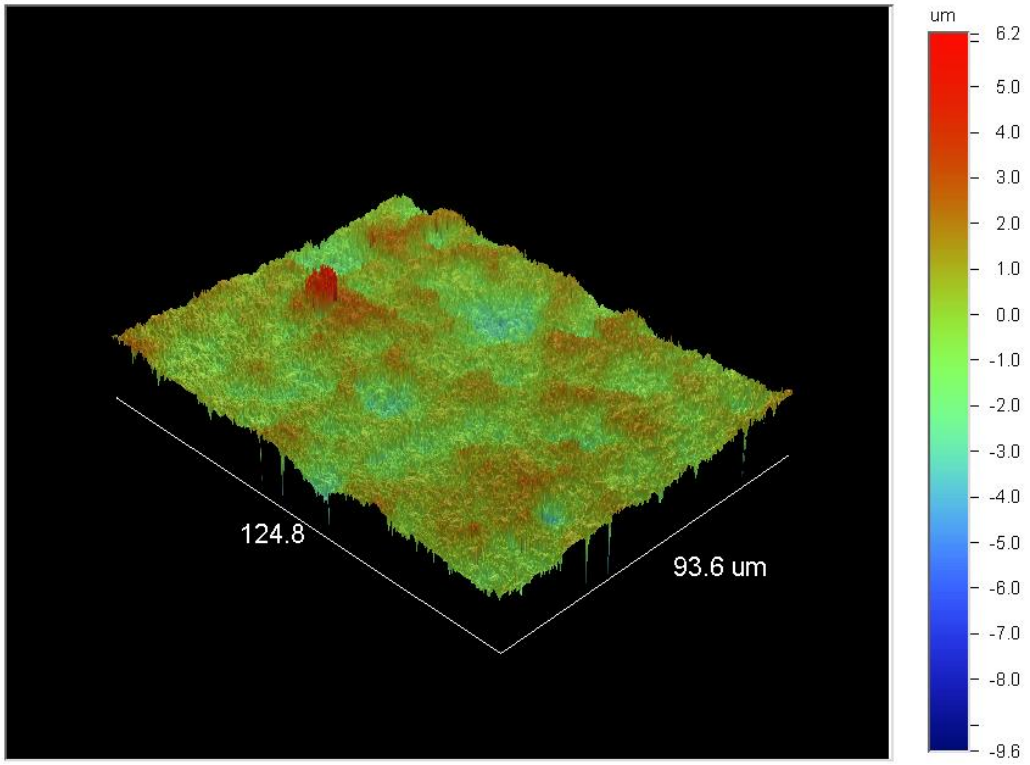

Figure 4.13: 3D Morphology 450 V, 50 sec

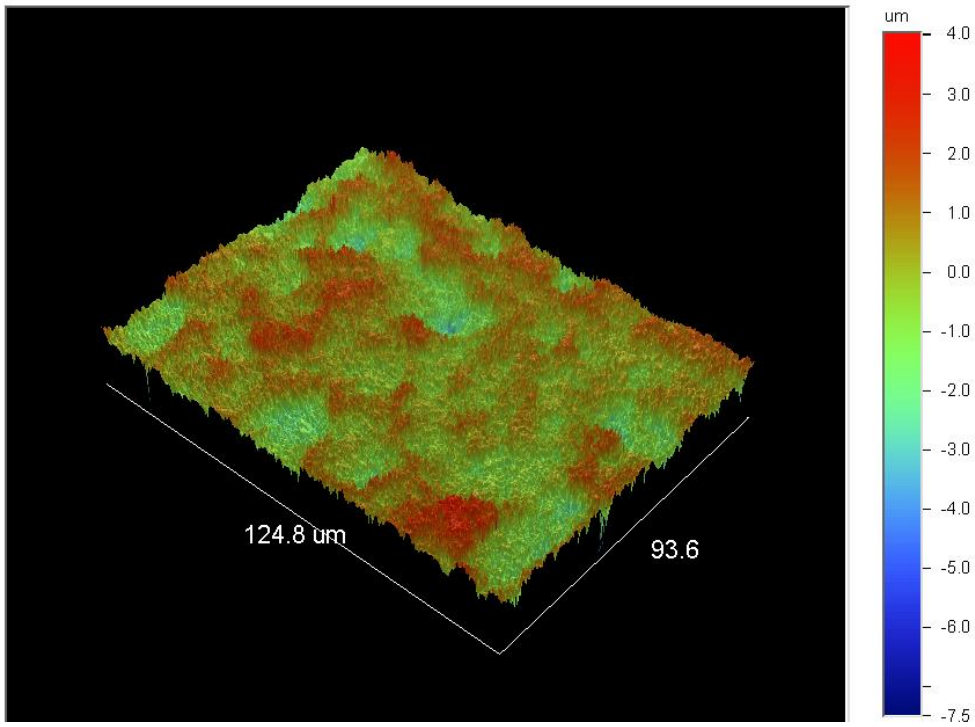

Figure 4.14: 3D Morphology 450 V, 100 sec

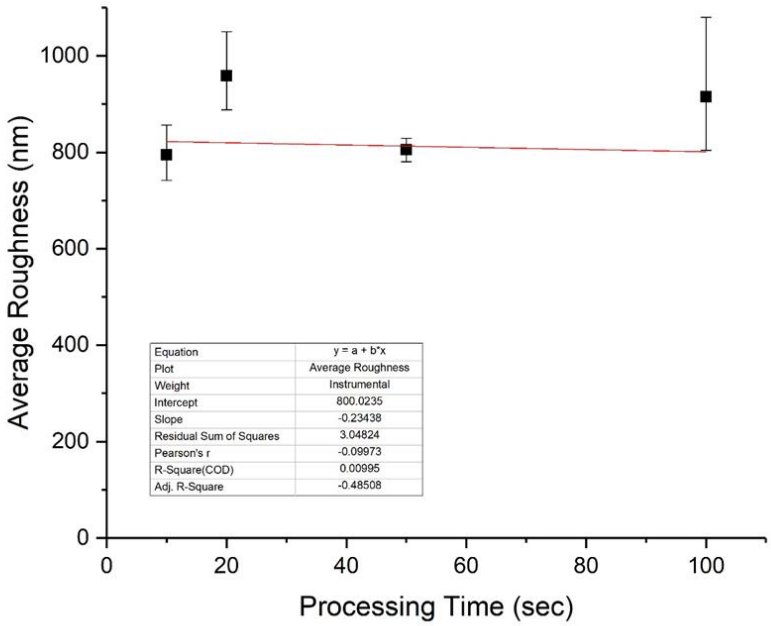

Figure 4.15: Roughness vs. Processing Time for Samples Processed at 450 V

The 3D plots were useful in illustrating the smoothness of the coated surface, with even the largest difference from maximum to minimum height being only about 15 µm. Roughness measurements were obtained 5 times from each sample, and the resulting ranges of roughness plotted above in Figure 4.15. When considering the similar 3D morphologies and the graph above, it cannot be concluded that adjusting the processing time has any effect on the coatings' surface morphology.

4.2.2 XRD Analysis

Next, the samples with the longest and shortest processing times were analyzed with an X-ray diffractometer, so that the composition of the coating and any differences in chemical composition based on processing time could be studied. The resulting data is shown below as Figure 4.16 and Table 4.2.

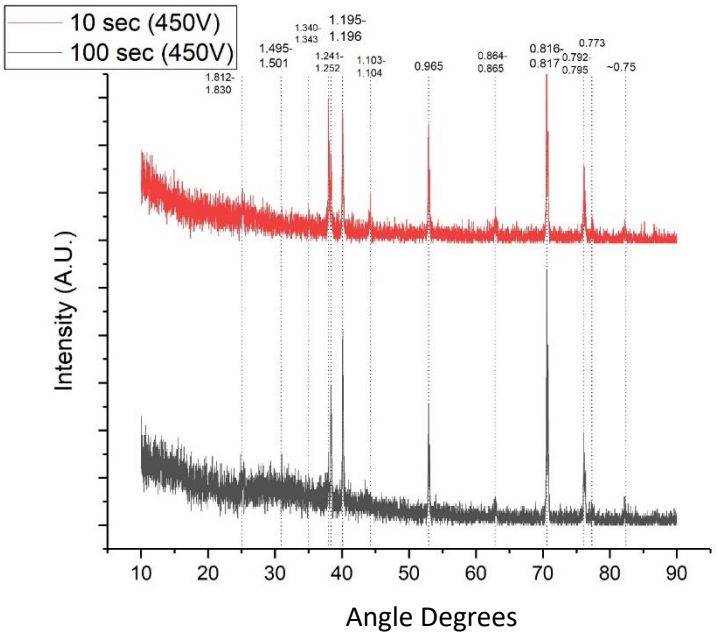

Figure 4.15: XRD of Samples Processed at 450 V for 10 and 100 sec

Table 4.2: Identified XRD Peaks and Their Possible Compounds

Experimental d(A)	Likely Compounds	Chemical Formula	Orientation	d(A)	2θ	(h,k,l)
1.821	Titanium Oxide	TiO2	Orthorhombic	1.830	49.785	(0,2,2)
	Titanium Phosphate	Ti4P6O23	Rhombohedral (R-Center)	1.830	49.785	(2,2,6)
	Titanium Oxide	Ti9O17	Triclinic	1.829	49.82	(0,0,16)
	Titanium Phosphide	P3Ti5	Orthorhombic	1.826	49.902	(2,3,2)
	Titanium Phosphide	TiP2	Unknown	1.824	49.96	unknown
	Phosphorus Oxide	P2O5	Orthorhombic	1.821	50.048	(4,4,0)
	Titanium Phosphide	Ti3P	Tetragonal	1.818	50.117	
	Titanium Pyrophosphate	TiP2O7	Cubic	1.818	50.137	(12,5,0)
	Titanium Phosphate	TiP2O7	Cubic (Unknown)	1.818	50.142	(12,4,3)
	Titanium Oxide	TiO2	Monoclinic	1.818	50.151	(0,1,3)
	Titanium Oxide	Ti7O13	Triclinic	1.812	50.317	(2,-2,12)
1.499	Titanium Oxide	TiO2	Monoclinic	1.501	61.736	(7,0,1)
	Titanium Phosphide	Ti3P	Tetragonal	1.501	61.724	(6,2,1)
	Titanium Phosphate	TiP2O7	Cubic (Unknown)	1.500	61.793	(12,10,2)
	Titanium Oxide	TiO2	Monoclinic	1.497	61.931	(-8,0,2)
	Phosphorus Oxide	P2O5	Orthorhombic	1.497	61.935	(4,4,2)
	Titanium Oxide	TiO2	Orthorhombic	1.497	61.935	(2,5,0)
	Titanium Oxide	Ti3O5	Monoclinic	1.496	61.981	(-4,2,0)
	Titanium Phosphide	TiP	Hexagonal	1.495	61.983	(2,0,1)
1.341	Rutile, syn	TiO2	Tetragonal	1.343	69.963	(1,1,2)
	Titanium Oxide	TiO	Unknown	1.341	70.116	unknown
	Phosphorus Oxide	P2O5	Unknown	1.340	70.176	unknown
	Titanium Phosphide	TiP	Hexagonal	1.340	70.147	(2,0,4)
1.25	Titanium Oxide	Ti8O15	Triclinic	1.252	75.932	(2,0,30)
	Titanium Oxide	TiO2	Orthorhombic	1.252	75.939	(3,1,2)
	Titanium Oxide	TiO2	Orthorhombic	1.252	75.903	(5,3,1)
	Titanium Phosphate	Ti3PO0.58	Orthorhombic	1.252	75.924	(2,0,4)
	Anatase, syn	TiO2	Tetragonal	1.250	76.017	(3,0,1)
	Phosphorus	P	Orthorhombic	1.250	76.082	(1,3,3)
	Phosphorus	P	Orthorhombic	1.250	76.045	(1,3,3)

	Phosphorus Oxide	P2O5	Unknown	1.250	76.082	unknown
	Titanium Oxide	Ti6O11	Triclinic	1.250	76.032	(4,0,22)
	Titanium Oxide	Ti7O13	Triclinic	1.249	76.125	(4,0,26)
	Titanium Oxide	Ti5O9	Triclinic	1.249	76.089	(1,2,4)
1.241	Rutile, syn	TiO2	Tetragonal	1.241	76.728	(2,0,2)
	Titanium Oxide	Ti6O11	Triclinic	1.241	76.69	(2,4,22)
1.196	Titanium Oxide	Ti8O15	Triclinic	1.196	80.172	(4,-4,14)
	Phosphorus Oxide	P2O5	Orthorhombic	1.196	80.188	(4,2,4)
	Titanium Oxide	Ti5O9	Triclinic	1.196	80.188	(3,-4,3)
	Titanium Oxide	TiO	Monoclinic	1.195	80.269	(-4,2,2)
	Titanium Oxide	Ti9O17	Triclinic	1.195	80.277	(4,-4,16)
1.103	Titanium Oxide	TiO2	Monoclinic	1.104	88.417	(-10,0,4)
	Titanium Oxide Phosphate	(TiO)2P2O7	Unknown	1.103	88.579	unknown
0.965	Rutile, syn	TiO2	Tetragonal	0.965	105.88	(3,2,2)
	Rutile, syn	TiO2	Tetragonal	0.965	105.9	(3,2,2)
	Titanium	Ti	Hexagonal	0.965	105.8	(2,1,0)
	Titanium	Ti	Hexagonal	0.965	105.8	(2,1,0)
	Titanium Oxide	TiO2	Monoclinic	0.965	105.88	(7,1,4)
	Titanium Oxide	TiO2	Tetragonal	0.965	105.79	(1,0,3)
0.865	Phosphorus	P	Orthorhombic	0.865	125.66	(0,2,5)
	Titanium Oxide	TiO2	Monoclinic	0.864	126	(2,2,6)
0.816	Rutile, syn	TiO2	Tetragonal	0.817	140.83	(5,2,1)
	Titanium Oxide	TiO2	Tetragonal	0.817	140.98	(3,1,3)
	Titanium Phosphide	TiP	Hexagonal	0.816	141.22	(2,0,12)
0.793	Phosphorus	P	Cubic	0.795	151.35	(3,0,0)
	Anatase, syn	TiO2	Tetragonal	0.792	152.62	(0,0,12)
0.773	Anatase, syn	TiO2	Tetragonal	0.792	152.62	(0,0,12)
	Rutile, syn	TiO2	Tetragonal	0.787	155.86	(5,3,0)
0.75	Phosphorus	P	Rhombohedral	0.764	---	(1,3,4)
	Phosphorus	P	Cubic	0.751	---	(3,1,0)
	Phosphorus	P	Cubic	0.715	---	(3,1,1)
	Titanium	Ti	Hexagonal	0.675	---	(1,1,4)
	Phosphorus	P	Cubic	0.661	---	(3,2,0)
	Phosphorus	P	Cubic	0.637	---	(3,2,1)

Comparing the experimentally obtained d-spacing with the closest values on the table, the following can be assumed about the composition of the coating. The first peak (d(Å) = 1.821) is probably indicative of Orthorhombic P_2O_5, which is made up of both of the most common ions present in the electrolyte but does not contain any titanium. This peak was very distinct on both samples, which suggests the phosphorus oxide formed quickly during processing and remained present throughout the entire process. The second peak at a d-spacing of 1.499 Å is most likely a peak for cubic TiP_2O_7. The presence of this crystalline compound is unique because it indicates that all three elements present in the coating surface can chemically bind into singular compound at some point during the process. This peak, however, was not significantly pronounced in the 10 second sample, which may indicate that this more complex compound only forms if given an extended amount of time during processing. The third peak likely indicates the formation of an unknown orientation of TiO (d(Å) = 1.341). Titanium monoxide is one of the lesser favorable oxides for titanium given that it makes titanium take a 4+ oxidation state. This is confirmed by the relatively short peak that is only pronounced at the shorter processing time, because it likely changes to a more favorable oxide given a longer time to process. The compounds for peaks 4 and 5 were so pronounced and close together in d-spacing that a tall bidentate peak formed. For peak 4 at 1.250 Å, there are many compounds with the exact same d-spacing. However, tetragonal anatase (TiO_2) is one of the most common and stable forms of titanium oxide, so it is safe to assume that with such a pronounced peak, anatase is likely the compound present. Peak 5 had a d-spacing of 1.241 Å, which for the same reasoning as with peak 4, is likely tetragonal rutile due to the size of the peak and stability of the oxide. The switch that occurs between whether peak 4 or 5 is taller at different processing times likely means that anatase can be formed in large amounts very quickly in the process but favors a slightly more stable rutile if given a longer time to process. The 6^{th} peak

(d(Å) = 1.196) is significantly taller than most of the other peaks and becomes even larger with a longer process. It is likely a sign of orthorhombic P_2O_5 because the other competing compounds are all less common crystal formations of titanium oxide. This would also explain the increase in the peaks size with longer processing time as more phosphorus and oxygen ions enter the surface coating. Peak 7 is another example of a compound present in the sample with a shorter processing time, but almost entirely vanished for the longer sample. A d-spacing of 1.103 Å probably indicates the presence of monoclinic titanium dioxide, which would also illustrate why the peak disappears, as the more stable titanium oxides would have been more favorable with a longer processing time. Peak 8 is consistent with very little change between the samples. At a d(Å) of 0.965, the most probable crystalline structure present is pure hexagonal titanium. Pure titanium likely contributes to several of the tallest peaks, because with a coating between 1-2 microns the x-rays are likely to penetrate the coating and yield several tall pure titanium peaks including this one. Peak 9 (d(Å) = 0.865) was smaller than most, but clearly present in both samples. For this reason, the most likely compound represented by this peak is pure orthorhombic phosphorus. The presence of unreacted phosphorus does not come as a huge surprise, because many of the largest peaks represent the formation of titanium oxide, which would leave surrounding phosphorus ions unreacted in regions with large amounts of TiO_2. Peak 10, located at a d-spacing of 0.816 Å, is the largest peak on the graph. Given the available options on the table, the most probable formation is that of tetragonal rutile (TiO_2). It is the most stable and favorable oxide of titanium and, like the peaks indicate, would increase in height with a longer processing time. Starting with peak 11 and onward, the number of available potential compounds to match the peaks significantly decreased and as a result the distance between the experimental d-spacings and the theoretical d-spacings increased. Peak 11 is located at 0.793 Å, and with its relative height compared to the other peaks below 0.8 Å, it

is likely that anatase is the compound represented by this peak as well. There are two equally probable possibilities as to which compound is represented by peak 12. The d-spacing of 0.773 Å is closer to rutile's nearest peak of 0.787 Å . However, the other option being anatase is also likely, because the much larger peak directly next to peak 12 is also probably anatase, so peak 12 could be a small variation off of peak 11. Finally, the last peak has a d-spacing of 0.75 Å, which is much closer to the value expected of cubic phosphorus than that of any other compound.

4.2.3 SEM & EDS Analysis

Below are the SEM images and EDS line scans obtained from the Hitachi S-3000 SEM for the cross-sectioned and mounted samples at 450 V and various processing times.

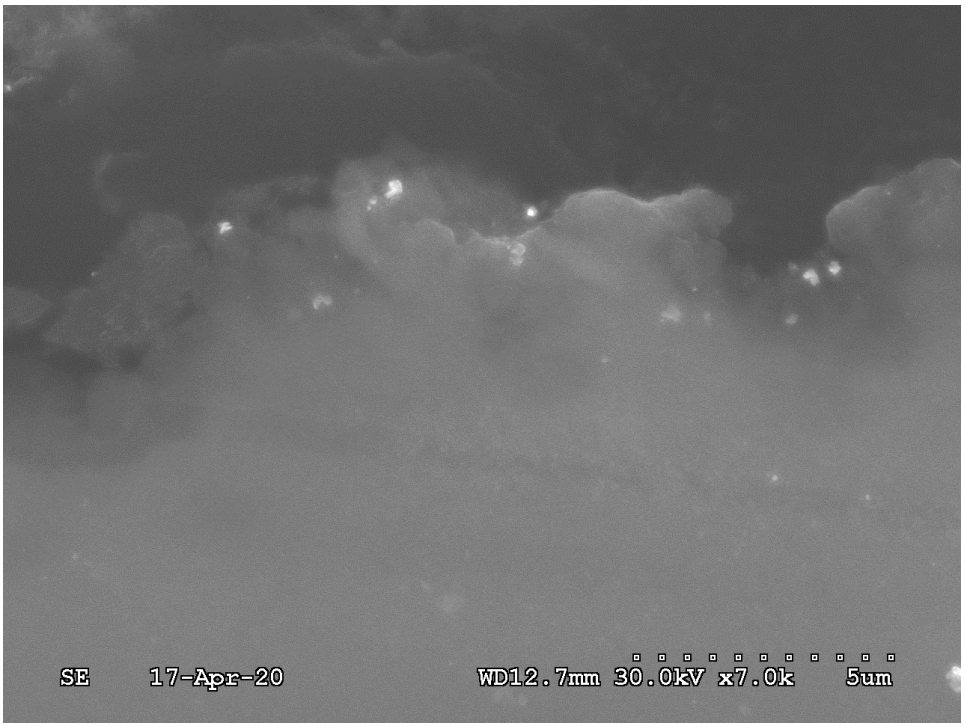

Figure 4.16: SEM Cross-Section for 450 V, 10 sec

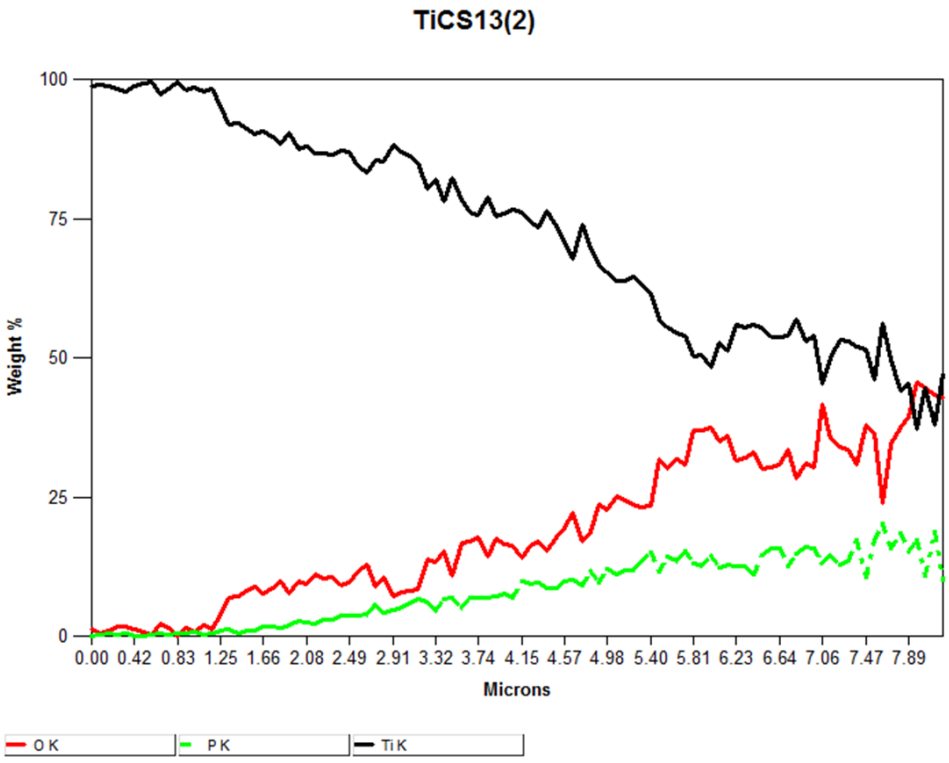

Figure 4.17: EDS Line Scan for 450 V, 10 sec

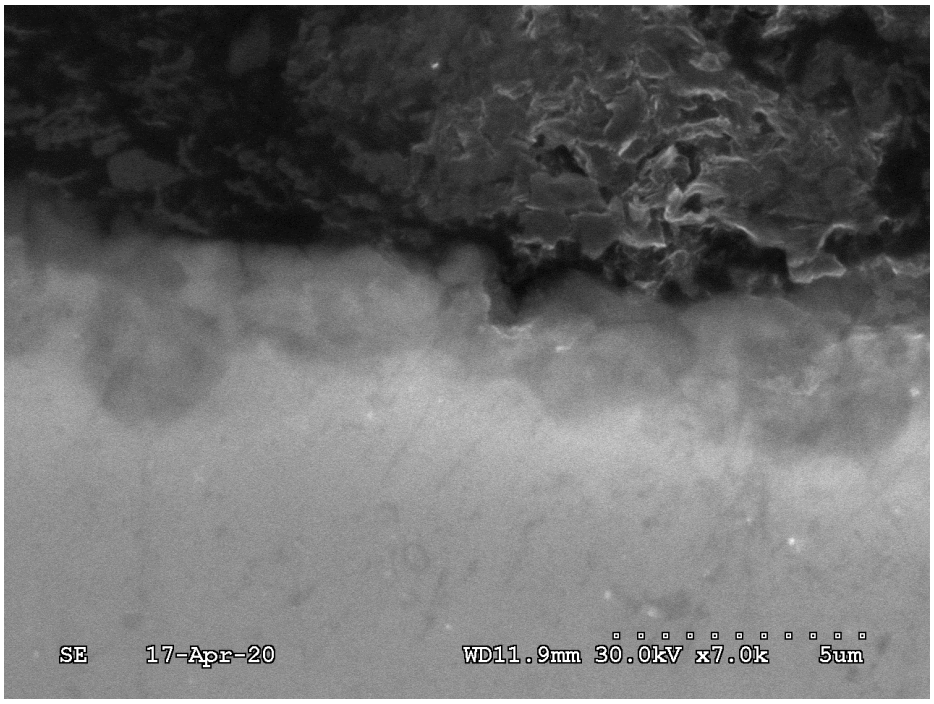

Figure 4.18: SEM Cross-Section for 450 V, 20 sec

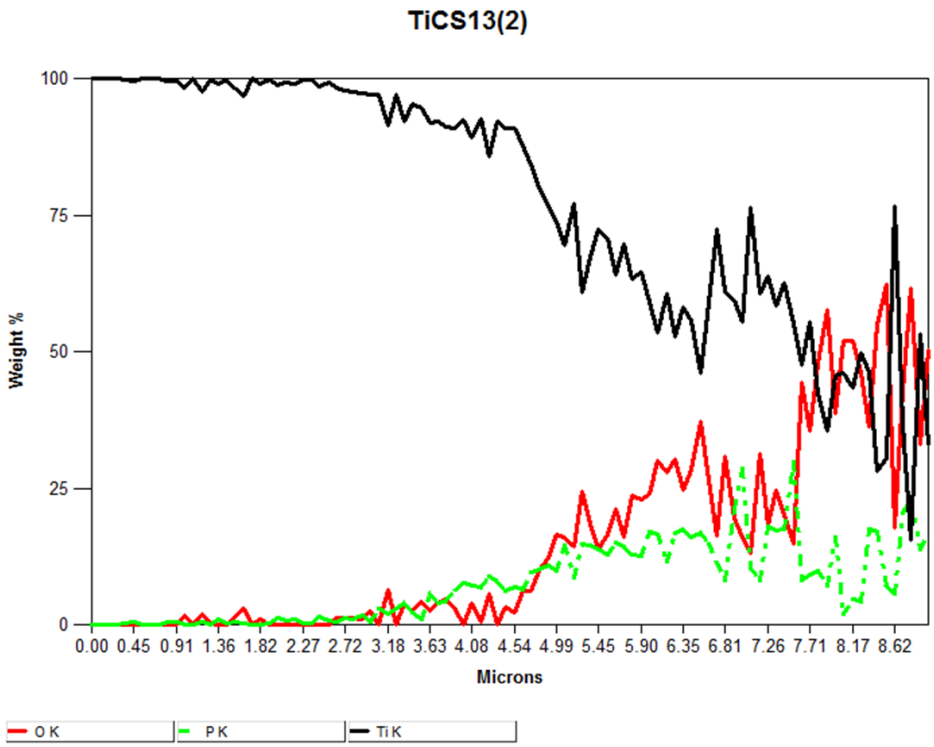

Figure 4.19: EDS Line Scan for 450 V, 20 sec

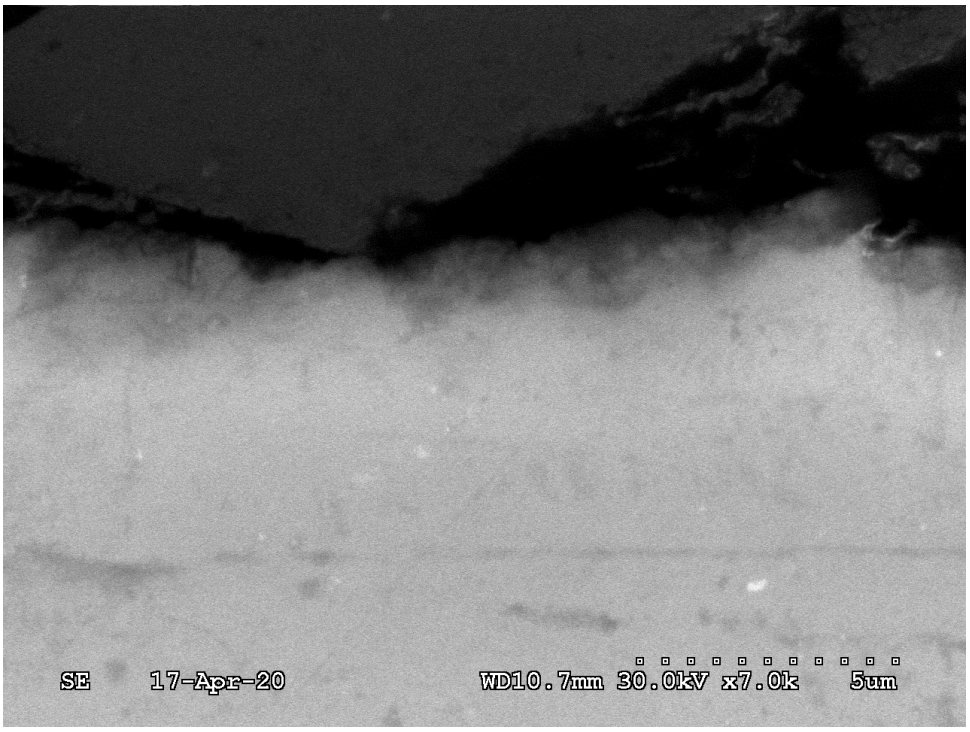

Figure 4.20: SEM Cross-Section for 450 V, 50 sec

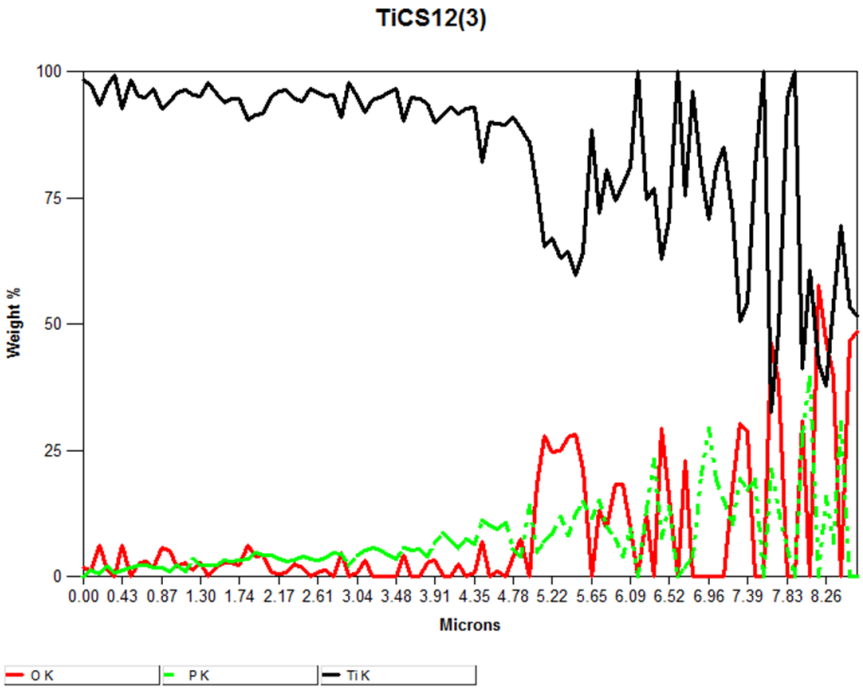

Figure 4.21: EDS Line Scan for 450 V, 50 sec

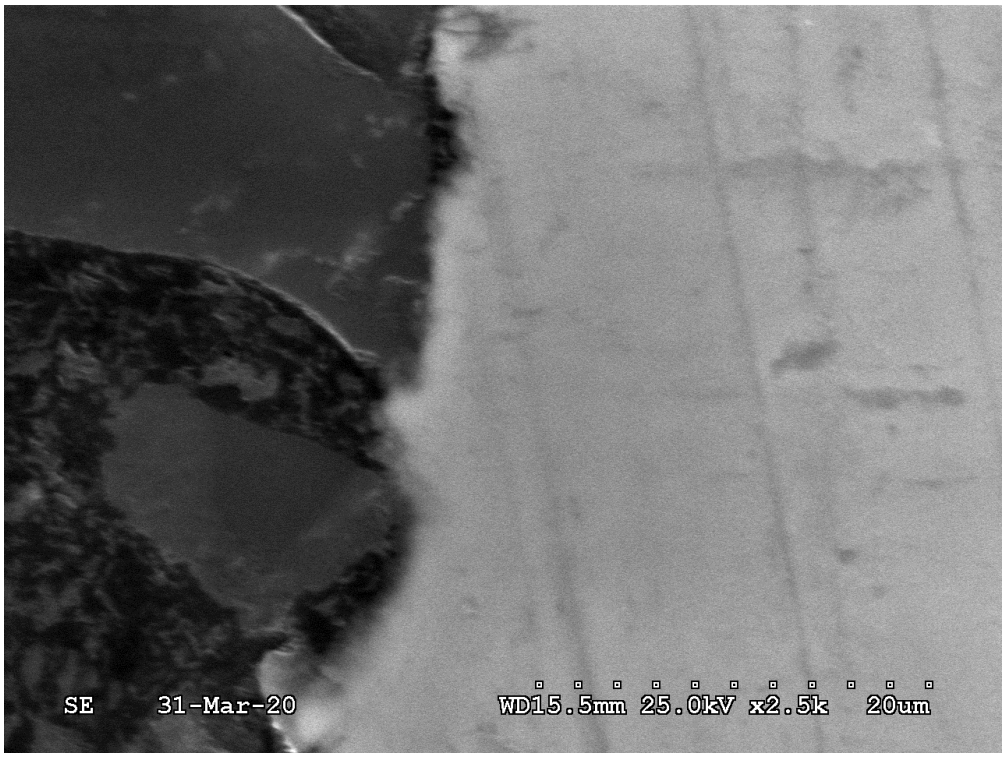

Figure 4.22: SEM Cross-Section for 450 V, 100 sec

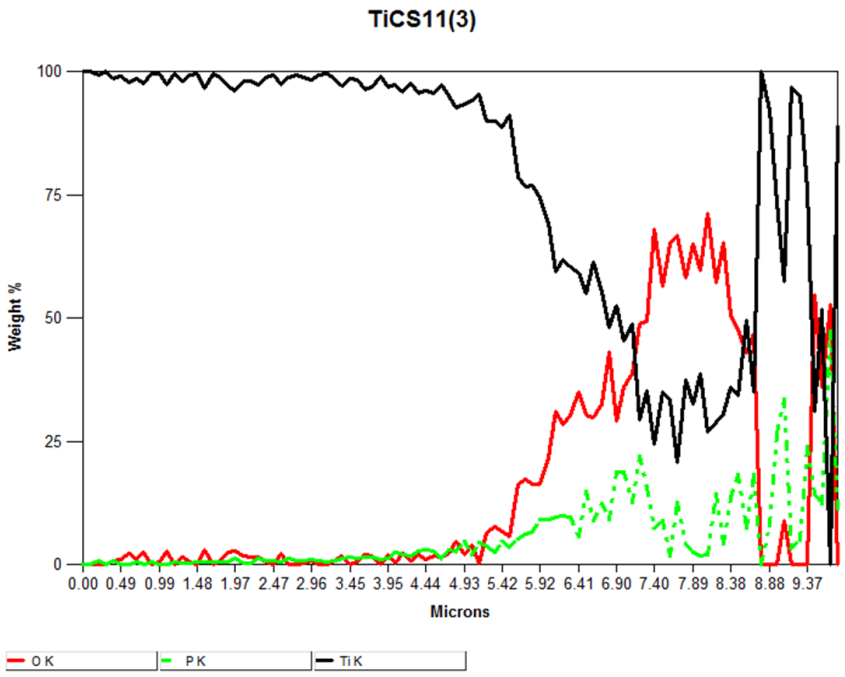

Figure 4.23: EDS Line Scan for 450 V, 100 sec

The lack of features ended up being detrimental to the quality of images that could be obtained using the Hitachi S-3000. As a result, the images obtained through this method appear fuzzy and unfocused. What can be deciphered from these results, is that the coating thickness for all four samples ranges from about 1-2 µm. The EDS results also showed a degree of variability that was unfortunate, but as with the SEM imagery, some conclusions could be drawn from them despite the issues. The EDS results all indicate that the amount of oxygen present in the coating portions of the cross-sections is greater than that of phosphorus, so this method of coating application is likely more favorable to oxygen ions than the phosphorus ions. This could also be caused by the fact that far more oxygen ions are present in the electrolyte than phosphorus. The FIB was then utilized to ensure that higher quality images of the coating were taken. To compare both processing time and operating voltage effects, FIB images were taken at various voltages as well as processing times. These high-definition images are shown below.

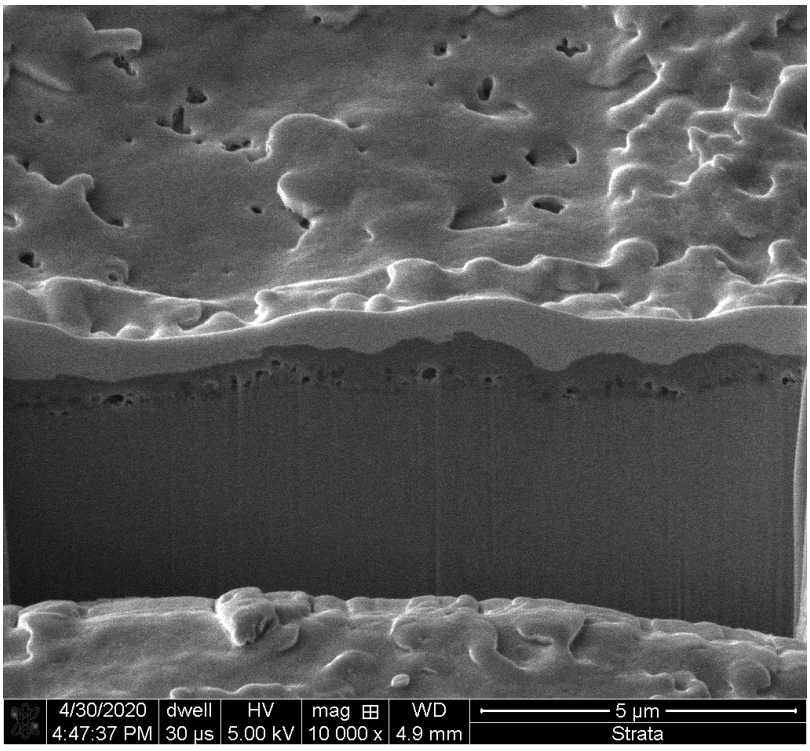

Figure 4.24: Cross-Sectional View 350 V, 100 sec

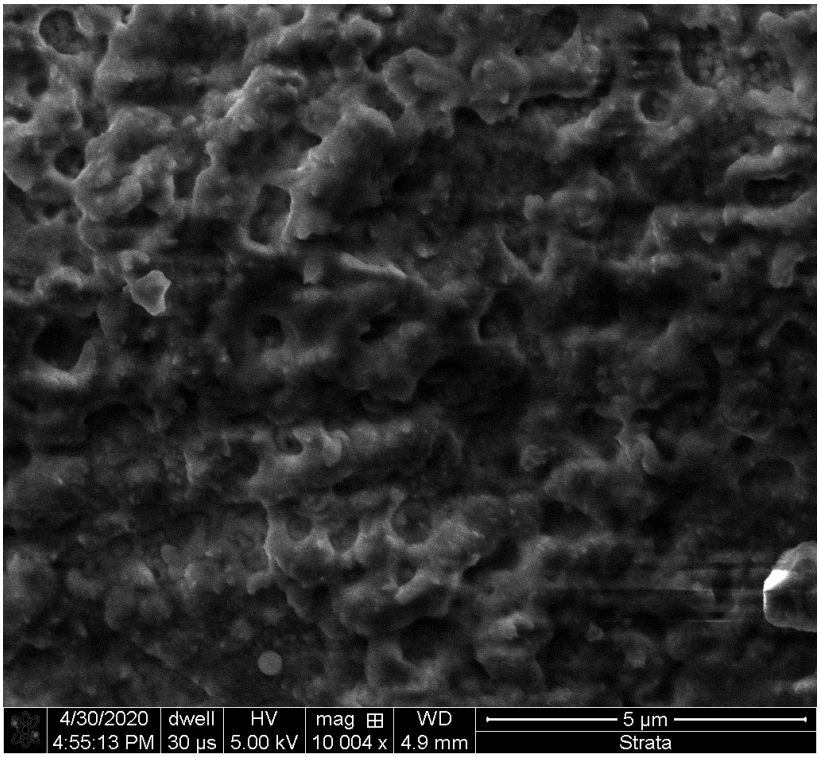

Figure 4.25: Topographical View 350 V, 100 sec

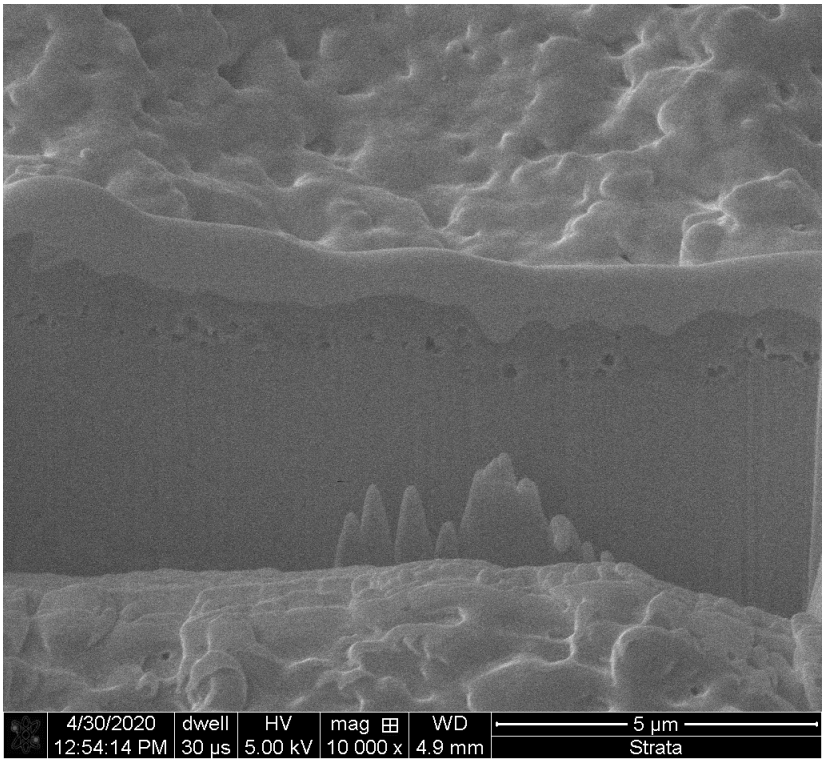

Figure 4.26: Cross-Sectional View 400 V, 10 sec

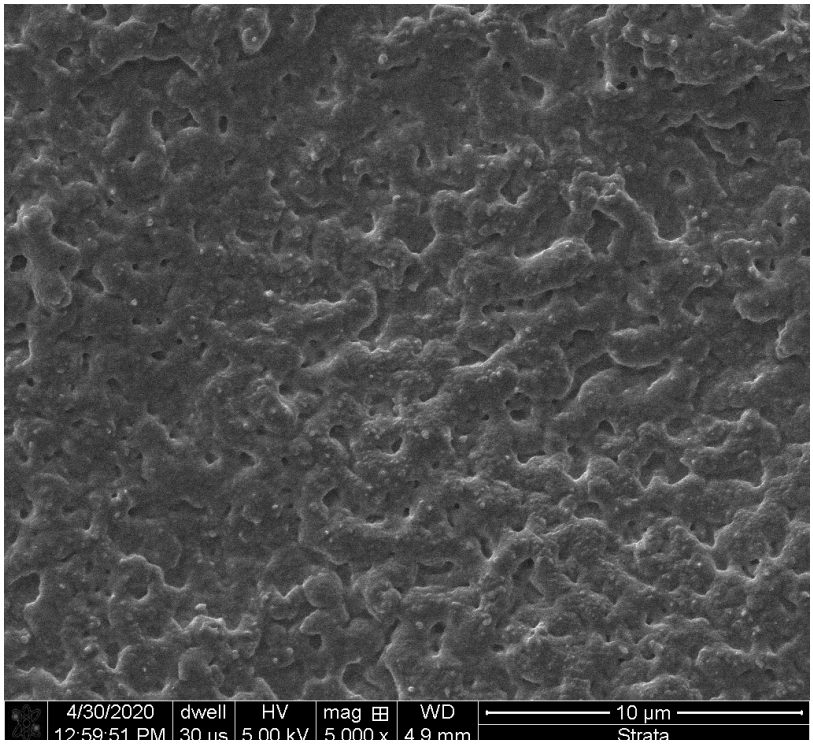

Figure 4.27: Topographical View 400 V, 10 sec

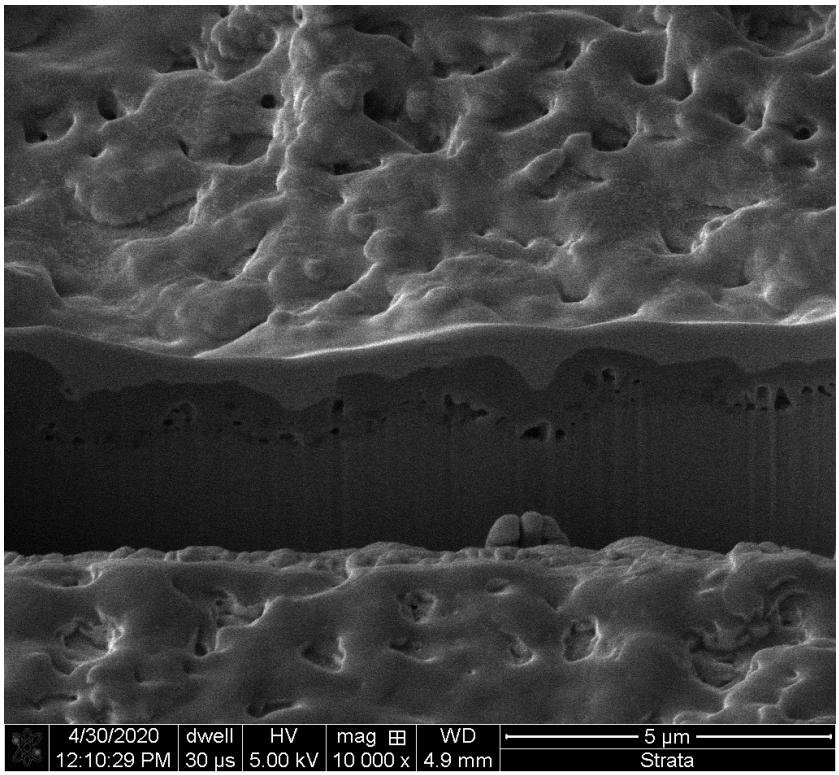

Figure 4.28: Cross-Sectional View 400 V, 20 sec

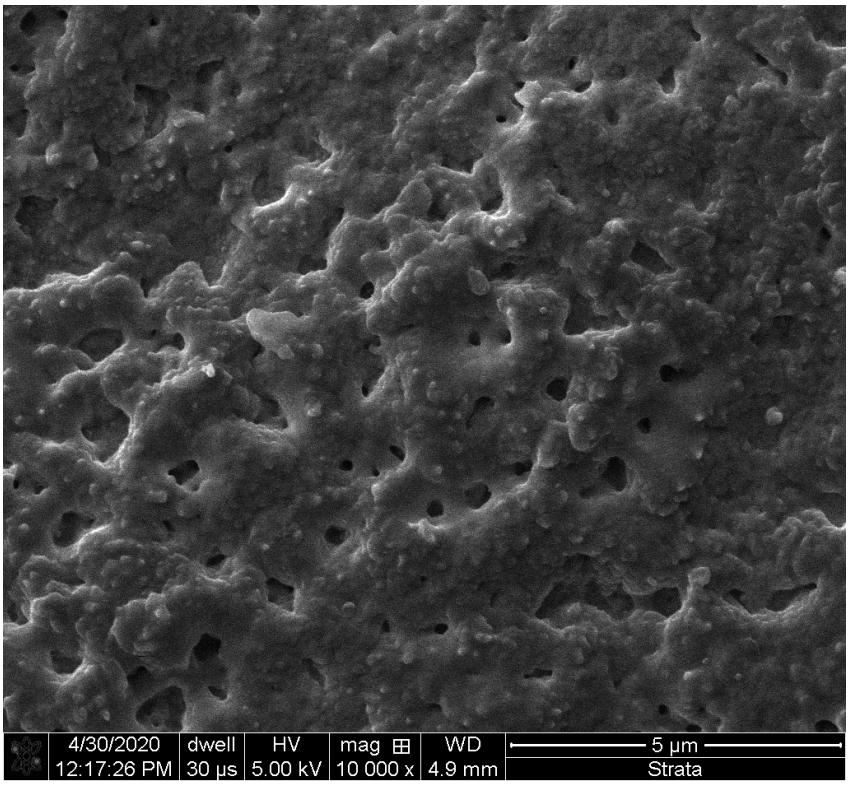

Figure 4.29: Topographical View 400 V, 20 sec

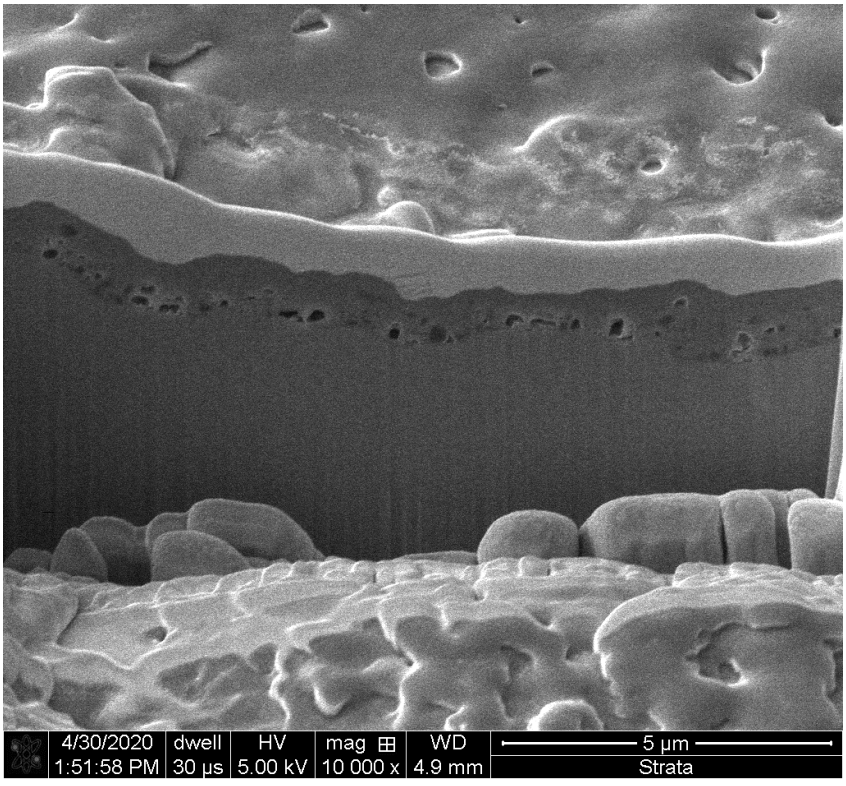

Figure 4.30: Cross-Sectional View 400 V, 50 sec

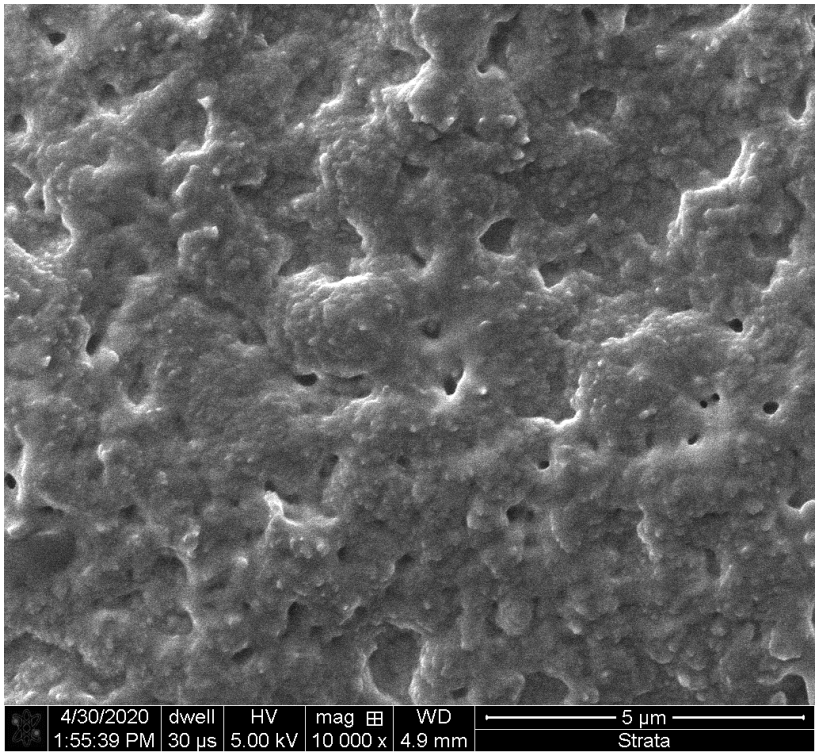

Figure 4.31: Topographical View 400 V, 50 sec

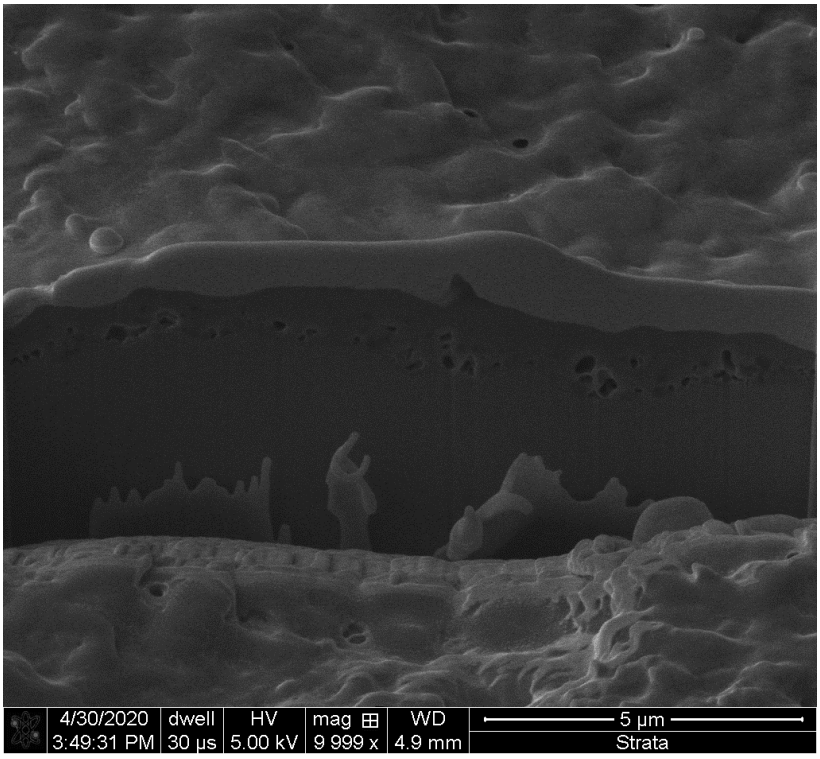

Figure 4.32: Cross-Sectional View 400 V, 100 sec

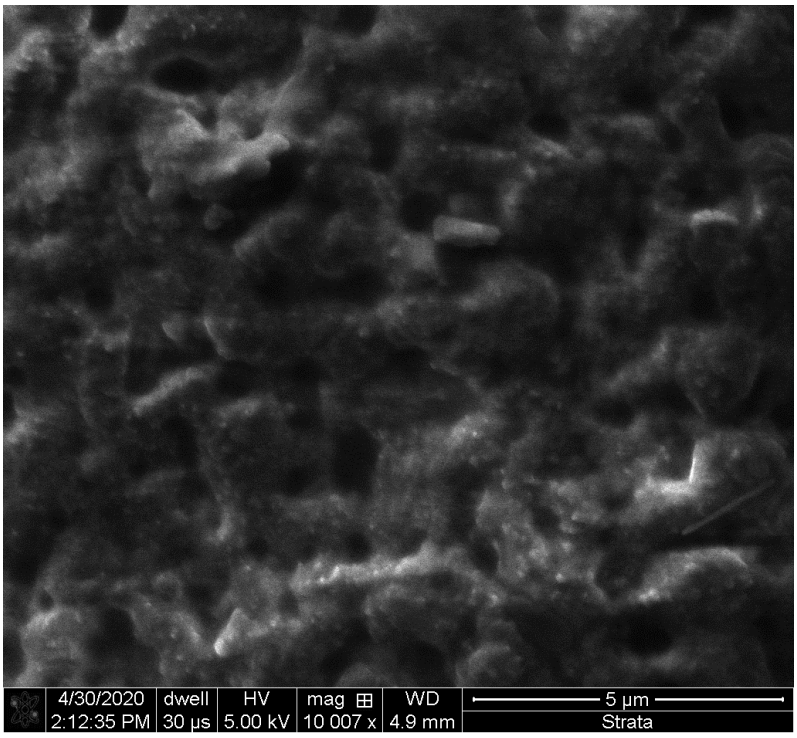

Figure 4.33: Topographical View 400 V, 100 sec

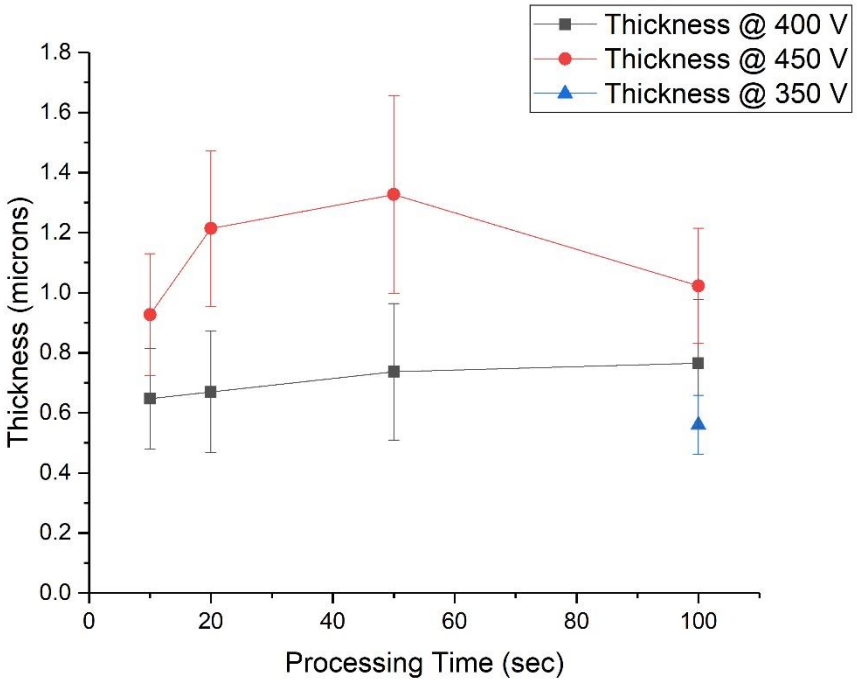

Figure 4.34: Thickness vs. Processing Time at Varied Processing Voltages

Figure 4.34 shows the results of the thickness measurements taken from samples processed at 350, 400, and 450 V. This graph shows, as expected, that beyond the 25-30 second decay of ionic current density that there is no significant increase in coating thickness. For the 400 V samples, the critical coating thickness was never reached, so arcing did not occur and there is no decrease in thickness. For 450 V, the critical coating thickness was reached after 50 seconds. This led to intense arcing on the surface of the substrate which caused the destruction of part of the

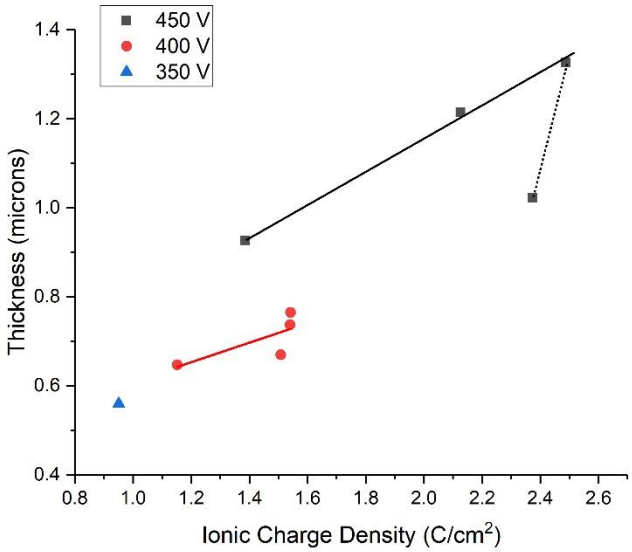

Figure 4.35: Thickness vs. Ionic Charge Density

coating as indicated by the decrease in thickness for 100 seconds. Figure 4.35 shows the near linear increase of thickness caused by increasing ionic charge. As shown in figure 4.34, after 50 seconds at 450 V there was intense arcing at the surface which caused the degradation of the surface coating. This caused the thickness of the coating at 100 seconds to no longer represent the linear relationship. This graph also shows that the coating thickness increases with increasing ionic charge density.

CHAPTER 5

CONCLUSIONS

- The present research revealed that current density is larger and allows for longer processing at higher constant processing voltages.
- It was found that majority of the coating applied through the PEO process is applied in the first 5 seconds.
- This research illustrated that by about 30 seconds, the current density is so low that continued processing has very minimal effect on the coating applied.
- It was discovered that the roughness of coatings applied with the PEO method do not show significant changes in surface roughness with different processing times.
- The chemical composition of the applied coating was shown to be primarily made up of the common titanium oxides anatase and rutile, but also contained sections of pure titanium, pure phosphorus, phosphorus oxide, and titanium phosphate.
- The coating formed showed clear signs of containing significantly larger amounts of oxygen than phosphorus.
- Processing time beyond 20 seconds likely has no effect on oxide thickness. Oxide thickness is more likely manipulated by changing the processing voltage under these conditions.
- Thickness was shown to increase linearly with ionic charge density until the critical thickness is reached. After that point intense arcing occurs on the surface and the coating is degraded.

REFERENCES

[1] Jouanny, I., Labdi S., Aubert P., Buscema C., Maciejak O., Berger M. -H., Guipont V., and Jeandin M. “Structural and Mechanical Properties of Titanium Oxide Thin Films for Biomedical Application.” Thin Solid Films, vol. 518, no. 12, 2010, pp. 3212–3217., doi:10.1016/j.tsf.2009.09.046.

[2] Mortazavi, Golsa. “Investigation of the Plasma Electrolytic Oxidation Mechanism of Titanium.” The University of Texas at Arlington, 2017.

[3] Kim, H., Koh Y., Li L., Lee S., and Kim H. “Hydroxyapatite Coating on Titanium Substrate with Titania Buffer Layer Processed by Sol–Gel Method.” Biomaterials, vol. 25, no. 13, 2004, pp. 2533–2538., doi:10.1016/j.biomaterials.2003.09.041.

[4] Chen, Jim-Shone, Horng-Yih Juang, and Min-Hsiung Hon. “Calcium Phosphate Coating on Titanium Substrate by a Modified Electrocrystallization Process.” Journal of Materials Science: Materials in Medicine, vol. 9, no. 5, 1998, pp. 297–300., doi:10.1023/a:1008825926440.

[5] Kasalica, B., Radic-Peric J., Peric M., Petkovic-Benazzouz M., Belca I., and Sarvan M. “The Mechanism of Evolution of Microdischarges at the Beginning of the PEO Process on Aluminum.” Surface and Coatings Technology, vol. 298, 2016, pp. 24–32., doi:10.1016/j.surfcoat.2016.04.044.

[6] Darband, Gh. Barati, Aliofkhazraei M., Hamghalam P., and Valizade N. “Plasma Electrolytic Oxidation of Magnesium and Its Alloys: Mechanism, Properties and Applications.” Journal of Magnesium and Alloys, vol. 5, no. 1, 2017, pp. 74–132., doi:10.1016/j.jma.2017.02.004.

[7] Zhang, W., Zhu Z., and Cheng C. “A Literature Review of Titanium Metallurgical Processes.” Hydrometallurgy, vol. 108, no. 3-4, 2011, pp. 177–188., doi:10.1016/j.hydromet.2011.04.005.

[8] Nemat-Nasser, S., Guo W. G., and Cheng J. Y. “Mechanical Properties and Deformation Mechanisms of a Commercially Pure Titanium.” Acta Materialia, vol. 47, no. 13, 1999, pp. 3705–3720., doi:10.1016/s1359-6454(99)00203-7.

[9] Murray, J. L., and H. A. Wriedt. “The O−Ti (Oxygen-Titanium) System.” Journal of Phase Equilibria, vol. 8, no. 2, 1987, pp. 148–165., doi:10.1007/bf02873201.

[10] Smith, Adam J. “Surface Modification of Iron and Aluminum by Electrolytic Plasma Processing.” The University of Texas at Arlington, 2014.

[11] Smith, A., Kelton R., and Meletis E. I. “Deposition of Ni Coatings by Electrolytic Plasma Processing.” Plasma Chemistry and Plasma Processing, vol. 35, no. 6, 2015, pp. 963–978., doi:10.1007/s11090-015-9642-9.

[12] Mortazavi G., Jiang J., and Meletis E. I. “Investigation of the Plasma Electrolytic Oxidation Mechanism of Titanium.” Applied Surface Science, vol. 488, 2019, pp. 370–382., doi:10.1016/j.apsusc.2019.05.250.

[13] Barati, Nastaran. “An Investigation of the Plasma Electrolytic Oxidation Mechanism for Coating of Alumina-Zirconia Nanocomposite.” The University of Texas at Arlington, 2018.

[14] Matykina, E., Berkani A., Sheldon P., and Thompson G. E. “Real-Time Imaging of Coating Growth during Plasma Electrolytic Oxidation of Titanium.” Electrochimica Acta, vol. 53, no. 4, 2007, pp. 1987–1994., doi:10.1016/j.electacta.2007.08.074.

[15] Ma X., Blawert C., Hoche D., Kainer K. U., and Zheludkevich M. L. “A Model Describing the Growth of a PEO Coating on AM50 Mg Alloy under Constant Voltage Mode.” Electrochimica Acta, vol. 251, 2017, pp. 461–474., doi:10.1016/j.electacta.2017.08.147.

[16] Shokouhfar, M., Dehghanian, C., Montazeri, M., Baradaran, A. “Preparation of Ceramic Coating on Ti Substrate by Plasma Electrolytic Oxidation in Different Electrolytes and Evaluation of Its Corrosion Resistance: Part II.” Applied Surface Science, vol. 257, no. 7, 2011, pp. 2617–2624., doi:10.1016/j.apsusc.2010.10.032.

[17] Jung, Y.C., Shin, K.R., Ko, Y.G., Shin, D.H. “Surface Characteristics and Biological Response of Titanium Oxide Layer Formed via Micro-Arc Oxidation in K3PO4 and Na3PO4 Electrolytes.” Journal of Alloys and Compounds, vol. 586, 2014, doi:10.1016/j.jallcom.2013.01.060.

[18] Venkateswarlu, K., Rameshbabu, N., Sreekanth, D., Sandhyarani, M., Bose, A.C., Muthupandi, V., and Subramanian, S. “Role of Electrolyte Chemistry on Electronic and in Vitro Electrochemical Properties of Micro-Arc Oxidized Titania Films on Cp Ti.” Electrochimica Acta, vol. 105, 2013, pp. 468–480., doi:10.1016/j.electacta.2013.05.032.

[19] Meletis, E.I., Nie, X., Wang, F.L., and Jiang, J.C. “Electrolytic Plasma Processing for Cleaning and Metal-Coating of Steel Surfaces.” Surface and Coatings Technology, vol. 150, no. 2-3, 2002, pp. 246–256., doi:10.1016/s0257-8972(01)01521-3.

[20] Hussein, R.O., Nie, X., Northwood, D.O., Yerokhin, A., and Matthews, A. “Spectroscopic Study of Electrolytic Plasma and Discharging Behaviour during the Plasma Electrolytic Oxidation (PEO) Process.” Journal of Physics D: Applied Physics, vol. 43, no. 10, 2010, p. 105203., doi:10.1088/0022-3727/43/10/105203.

BIOGRAPHICAL INFORMATION

In 2018, Joshua Twaddle graduated from Texas Tech University with a B.S. degree in Chemistry. During his time at TTU he worked under Dr. Whittlesey synthesizing specific amino acid chains, and under Dr. Hope-Weeks studying the epoxidation of Tungsten Chloride to create aerogels. After graduating, Joshua began pursuing an M.S degree in Materials Science and Engineering from the University of Texas at Arlington.